PKM2-EZH2 INTERACTION ELICITS METABOLIC VULNERABILITY FOR TREATMENT OF TRIPLE- NEGATIVE BREAST CANCER

by

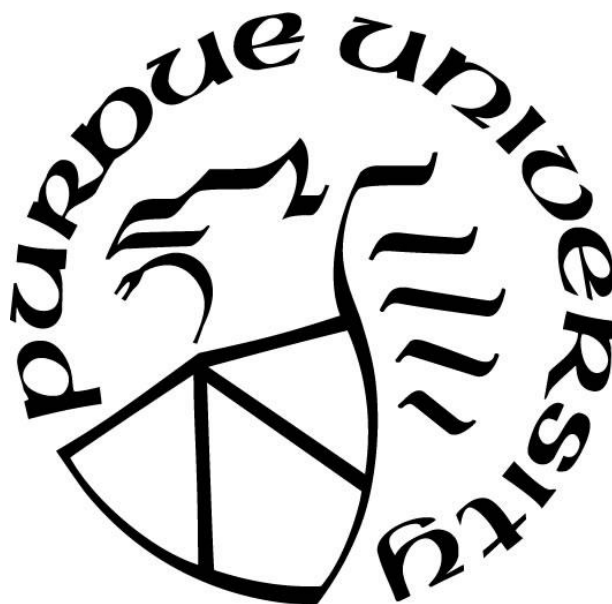**Yingsheng Zhang**

A Dissertation

Submitted to the Faculty of Purdue University

In Partial Fulfillment of the Requirements for the degree of

Doctor of Philosophy

Department of Animal Sciences

West Lafayette, Indiana

May 2020

THE PURDUE UNIVERSITY GRADUATE SCHOOL
STATEMENT OF COMMITTEE APPROVAL

Dr. Alice Chang, Co-Chair

    Roswell Park Cancer Institute

Dr. Shihuan Kuang, Co-Chair

    Department of Animal Science

Dr. Michael Wendt

    Department of Medicinal Chemistry and Molecular Pharmacology

Dr. Guangjun Zhang

    Department of Comparative Pathobiology

Approved by:

    Dr. Jason R. Cannon

        Head of the Graduate Program

ACKNOWLEDGMENTS

During my four years graduate study at Purdue University, many people helped me a lot. First and foremost, I would like to thank Dr. Alice Chang, who is one of two co-advisors of my thesis. She always encouraged me to think big in science. She pushed me forward when I settled, and she encouraged when I felt frustrated. She helped not only in research but also in life. Next, I would like to thank Dr. Shihuan Kuang, who is the other co-advisor of my thesis. I really appreciated that he allowed me to do experiments in his lab last summer in which Alice was relocating from Purdue to Roswell. Dr. Kuang not only helped me to deal with lots of annoying administrative procedures in the last year, but also gave me many insightful research and career suggestions. Moreover, I would like to thank all my thesis committee members along the way, Dr. Alice Chang, Dr. Shihuan Kuang, Dr. Michael Wendt, Dr. Guangjun Zhang and Dr. Jer-Yen Yang. It was my great honor to have such a great thesis committee. Without their tutorship, I can never finish my thesis research. All of them were always more than happy to answer any questions about my research and career. Their passion to science, insightful ideas, and professionalism really inspired me a lot. Meanwhile, I would like to thank my lab mates in Dr. Alice Chang's lab, Dr. Meng-Ju Wu, Dr. Mi Ran Kim, Dr. Silpa Gampala, Dr. Robert V Robin Swamidoss, and Yueyang Wang. I will always cherish the working and life experience with them. Furthermore, I feel so fortunate being a graduate student in PULSe program at Purdue University. It is and will always be one of most precious experiences in my life. I thank everyone I met at Purdue, my friends, my teachers, the staff at Purdue, and many more. Finally, I would like to give the biggest thanks to my family. Thank my parents and my sisters for always supporting and understanding me.

TABLE OF CONTENTS

LIST OF FIGURES

ABSTRACT

Triple Negative Breast Cancer (TNBC) is the most aggressive type of breast cancer. TNBC patients are resistant to virtually all target therapies and suffer a higher post-chemotherapy relapse with a worse overall survival compared with other types of breast cancers. Therefore, the development of an effective therapy is urgently needed. PKM2 plays a prominent role in mediating tumor glycolysis and PKM2 is often overexpressed in human cancers. However, whether PKM2 mediated glycolysis is necessary for cancer cell growth is questionable. Here, I have found that inhibition of PKM2 does not affect TNBC cell growth due to a metabolic switch from glycolysis to fatty acid oxidation (FAO). We show that PKM2 directly interacts with EZH2 to coordinately mediate epigenetic silencing of SLC16A9, transporter of a key player in FAO, Carnitine. Inhibition of either PKM2 or EZH2 increases levels of SLC16A9 and intracellular Carnitine to promote FAO and thereby sustains cancer cell growth. Direct inhibition of EZH2 using a clinically tested EZH2 inhibitor, GSK126, is able to elicit a previously unidentified vulnerability to a clinically tested FAO inhibitor, Etomoxir. As a result, combined GSK126-Etomoxir treatment synergistically abolishes TNBC xenograft tumor growth in vivo. Together, this study uncovers PKM2-EZH2 mediated metabolic reprogramming that leads to a new drug combination therapy by dual targeting of EZH2 and FAO for effective treatment of TNBC.

Furthermore, Dendritic Cell (DC) vaccination has shown promise in treating cancer patients. However, the *in vitro* generation of a fully functional DC remains a big challenge in this field. EZH2 inhibition has shown to be able to create an immunologically 'hot' tumors. Nonetheless, the role of EZH2 in regulation of DC function is still unclear. I found that the expression levels of EZH2 and its functional maker, H3K27Me3, are enhanced following maturation from immature

DC (iDC) into two functional DCs, α-type 1-polarized-DC (αDC) and gold standard DC (sDC).

Moreover, inhibition of EZH2 by GSK126 treatment elicits a dependency of sDC on FAO. These

results suggest that EZH2 plays a role in maturation of DC through metabolic reprogramming,

which may also provide new DC based immunotherapy of TNBC.

CHAPTER 1.   INTRODUCTION

1.1   Motivation

Triple Negative Breast Cancer (TNBC), the most aggressive breast cancer subtype that lacks the expression of estrogen receptor (ER), progesterone receptor (PR), and human epidermal growth factor receptor 2 (HER2), is resistant to virtually all receptor targeted therapies, including Tamoxifen (targeting ER) and Trastuzumab (targeting HER2). Currently chemotherapy remains the first line treatment for TNBC; however, chemotherapy treated TNBC patients still suffer a higher relapse rate with a worse overall survival compared with other types of breast cancers (1–3). Therefore, there is an urgency for development of new and effective treatments for TNBC.

1.2   Background

Breast cancer is the most common cancer and the second leading cause of cancer death in women. Based on the expression of estrogen receptor (ER), progesterone receptor (PR), and human epidermal growth factor receptor 2 (HER2), breast cancer can be divided into three molecular subtypes, the luminal, the HER2+, and the basal/triple-negative breast cancer (TNBC) subtypes. Luminal type breast cancer expresses ER and/or PR, HER2+ breast cancer expresses HER2, while basal/TNBC lacks the expression of all these three proteins. Besides local therapy for breast cancer, such as surgical resection and radiation, different systemic therapies are administered to treat breast cancer patients according to their molecular subtypes to prevent progression and recurrence (*4*). Currently, endocrine therapy is the main systemic therapy for luminal type breast cancer patients. It consists of either directly inhibiting ER signaling through administration of tamoxifen or reducing the circulating estrogen by applying aromatase inhibitors (*5*). For HER2 breast cancer, the anti-HER2 therapy which includes the administration of either an anti-HER2 antibody, such as

Trastuzumab, or a small tyrosine kinase inhibitor, such as lapatinib and neratinib, that inhibit HER2 signaling and therefore hinder the proliferation of cancer cells (*4*, *6*). Because of a lack of expression of the hormone receptors, TNBC patients do not respond to the targeted therapies. The first line treatment for TNBC patients is still chemotherapy, including docetaxel or paclitaxel to disrupt mitosis, as well as cyclophosphamide or adriamycin to disrupt DNA replication (*2*, *4*, *7*, *8*). However, TNBC patients experience a higher relapse rate in the first 3 to 5 years after diagnosis compared to luminal and HER2 breast cancer patients (*2*). 5-year survival rate of TNBC patients is also much lower than the other two types of breast cancer patients (*9*). Furthermore, ~5% breast cancer patients carry germline mutations in breast cancer type 1 susceptibility proteins, BRCA1 and BRCA2, which are important for DNA damage repair. It has been shown that targeting the alternative DNA repair pathway mediated by poly (ADP-ribose) polymerase protein (PARP) in BRCA breast cancer can lead to synthetic lethality for effective treatment. Synthetic lethality indicates that disruption of either of the individual process does not have obvious effect while perturbation of both processes can cause significant cell death/growth inhibition (*10*). Two PARP protein inhibitors, olaparib and talazoparib, were approved in 2018 to treat refractory breast cancer patients who have BRCA mutations (*11*, *12*). However, this targeted therapy is only effective in ~5% BRCA mutated breast cancer patients; development of a new targeted therapy for the treatment of TNBC is still urgent and demanding.

Warburg effect is a hallmark of cancer. This phenomenon describes that even in the presence of oxygen, cancer cells still prefer to undergo glycolysis rather than oxidative phosphorylation; therefore, Warburg effect is also known as 'aerobic glycolysis'(*13*). The genes related to glycolysis are often upregulated in cancers, and among them, pyruvate kinase is particularly overexpressed.

Pyruvate kinase catalyzes the last step of glycolysis, from phosphoenolpyruvate (PEP) to pyruvate(*14*). There are three types of pyruvate kinase, Pyruvate Kinase Liver (PKL), Pyruvate Kinase Erythrocytes (PKR), and Pyruvate Kinase Muscle (PKM). PKL and PKR express in liver and erythrocytes, respectively, and PKM expresses in the other tissues. PKM has two isoforms, PKM1 and PKM2. These two isoforms have only one exon difference. PKM1 exclusively contains exon 9, and PKM2 uniquely has exon 10 (*15*) (Figure 1-1). In cancer cells, the main PKM isoform is PKM2, and the expression of PKM2 is necessary for sustaining the glycolytic phenotype and providing metabolic intermediates as building block molecules for biosynthesis to promote growth of cancer cells (*16*, *17*). In a steady state, PKM2 is in the dimerized form. When being allosterically activated by FBP, an upstream glycolytic intermediate, PKM2 becomes tetramerized and has a higher pyruvate kinase activity than being dimerized. In response to oncogenic signaling, such as tyrosine kinase signaling, PKM2 is mainly in the dimerized form and promotes the accumulation of the intermediates of glycolysis for the purpose of biosynthesis (*18–20*). It is widely accepted that dimerized PKM2 has various functions beyond its low pyruvate kinase activity. Dimerized PKM2 can enter into the nucleus and act as a protein kinase of transcription factors or histone H3 and also functions as a transcriptional coactivator to enhance the expression of genes related to glycolysis and proliferation to promote cancer progression (*21–25*). In breast cancer, a study showed that PKM2 expression is correlated with poor prognosis of TNBC patients and maintains the cancer stem cell population (*19*). Moreover, methylation of PKM2 by CARM1 is crucial for the balance of aerobic glycolysis and oxidative phosphorylation in breast cancer cell proliferation, migration and metastasis, suggesting an important role of PKM2 in breast cancer progression (*26*). However, there are also reports questioning whether the oncogenic role of PKM2 is dependent on its pyruvate kinase activity (*27–30*). It was reported that small molecules of PKM2 activators, such

as TEPP-46, which promoted the formation of PKM2 tetramerization, inhibited tumor growth in a preclinical H1299 lung cancer model (*31*), whereas TLN-232, a drug disrupted the formation of PKM2 dimer, failed to show benefits in a renal carcinoma clinical trial (*32*). It is likely that PKM2 can promote oncogenesis through a non-glycolytic function; however, the mechanism by which PKM2 uses to promote TNBC progression remains to be determined.
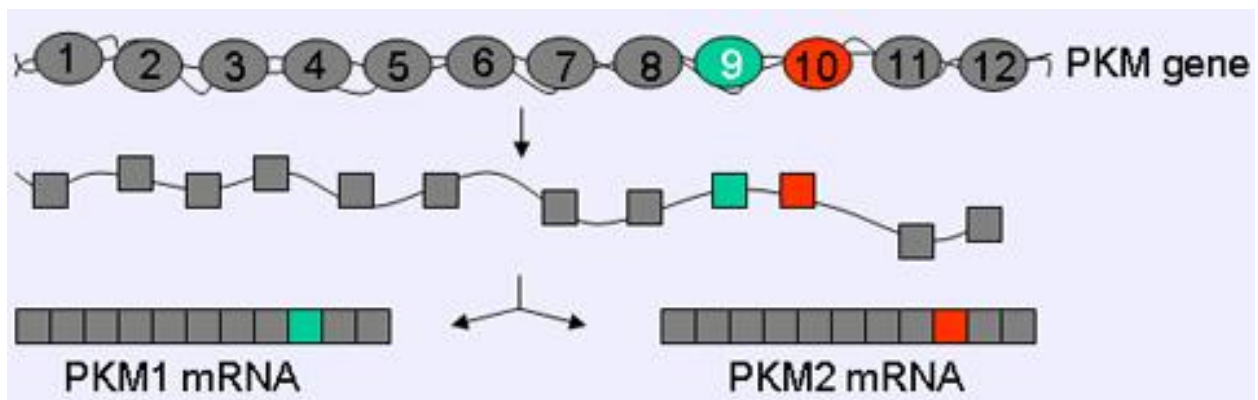
Figure 1-1: Alternative splicing of PKM that generates two isoforms, PKM1 and PKM2

Histone modification is an epigenetic regulation of gene expression which is irrelevant to DNA sequence (*33*). The post-translational modification of histone at its tail, including methylation, acetylation, phosphorylation, can either increase or decrease gene expression through regulating the accessibility of chromatin and change the transcriptome composition (*34*, *35*). Enhancer of zeste homolog 2 (EZH2), the enzymatic component of Polycomb Repressive Complex 2 (PRC2) that accounts for methylation of histone H3 at lysine 27 (H3K27Me3), a marker of transcriptional silencing of a cohort of target genes involved in embryonic development and tissue homeostasis (*36*, *37*). PRC2 itself cannot bind to DNA, however, it can be recruited to specific genomic loci by other factors, such as long non-coding RNAs (lncRNAs) (*38*). It has been shown that HOTAIR, a

lncRNA transcribed from HOXC cluster, can direct PRC2 to the HOXD cluster to repress gene expression (*39*). Moreover, Zhao *et al.* has discovered that lncRNA Xist can recruit PRC2 to one X chromosome and results in its inactivation in female germ cells (*40*). The association between EZH2 and lncRNAs is a dynamic process that can be influenced by EZH2 post-translational modifications. Kaneko *et al.* has revealed that the phosphorylation of Ezh2 by CDK1 at Thr345 and Thr487 increases its ability of binding to HOTAIR and Xist (*41*). EZH2 has six major domains, including (i) a WDB domain which binds to a PRC2 protein, Embryonic Ectoderm Development (EED), (ii) a SANT domain which interacts with H3, (iii) a D2 domain which associates with another PRC2 protein, Suppressor of Zeste 12 Protein Homolog (SUZ12), (iv) a non-coding RNA binding domain for EZH2 binding to non-coding RNAs, and (v) a CXC domain linked with (iv) a SET domain, both are critical for the methyltransferase activity (*42–44*) (Figure 1-2). EZH2 has been shown involved in the development and progression of many cancers. EZH2 is overexpressed in hormone-refractory metastatic prostate cancer and its overexpression is associated with poor prognosis. Reducing expression of EZH2 by siRNA in prostate cancer cells inhibits cell proliferation in vitro (*45*). In a systemic clinical study cross different cancer types, expression of EZH2 is uniformly and positively correlated with the tumor grade that can serve as a strong prognostic marker for patient survival in melanoma, prostate, and endometrial carcinoma (*46*). EZH2 is also found to be highly mutated in blood cancers. A sequencing study discovered that tyrosine mutation at 641 of EZH2 appeared in 21.7% of the GCB subtype of diffuse large B-cell lymphoma (DLBCL) and 7.2% of follicular lymphoma (FL) (*47*). This gain-of-function mutation results in overall increase of H3K27Me3 of the genome, and thus represses a bunch of genes expression (*48*, *49*). In breast cancer, EZH2 expression has been found to be positively associated with the incidence of breast cancer development (*50*, *51*), tumor aggressiveness, and patient

survival rate (*52–55*). Mechanistically, it has been found that EZH2 can silence the expression of cell cycle inhibitors, such as CDKN1C and RUNX3, to drive cell cycle progression (*56, 57*). EZH2 inhibits the expression of anti-metastatic genes, such as FOXC1, RKIP, and CDH1, to promote tumor invasion and metastasis (*58–60*). EZH2 also suppresses the expression of DNA repair gene, RAD51, to promote breast cancer stem cell traits (*61*). Although the versatile role of EZH2 in various cellular processes has been uncovered, it is still unclear whether and how EZH2 regulates the metabolism in breast cancer cells to promote cancer progression. Moreover, despite that there have been drugs developed targeting EZH2 to inhibit its methyltransferase activity, including Tazemetostat, GSK126, and CPI-1205, these drugs were mainly used for treatment of lymphomas while they did not yield seeming benefits in other solid tumors (*62*). Therefore, development of effective therapeutic strategies using new drug combination to enhance EZH2 inhibitor efficacy in solid tumors is necessary. Besides the role of EZH2 in cancer cells, there are also many studies showing the function of EZH2 in immune modulation. Dupage et. al. revealed that EZH2 was essential for stabilizing Foxp3 directed transcriptional program of Treg cells and ablation of EZH2 led to severe autoimmunity (*63*). Yang *et al.* also found that EZH2 deletion resulted in loss of Treg cells and increased numbers of T effector cells (*64*). Wang *et al.* and Goswami *et al.* further demonstrated that mice showed a stronger tumor immune response in Treg cells by genetically deletion of EZH2 or pharmacologically inhibition of EZH2, and that inhibition of EZH2 enhanced the efficacy of immune checkpoint therapy (*65, 66*). Despite the crucial role of EZH2 in Treg cells, the function of EZH2 in other types of immune cells, such as dendritic cells (DC), is still elusive.
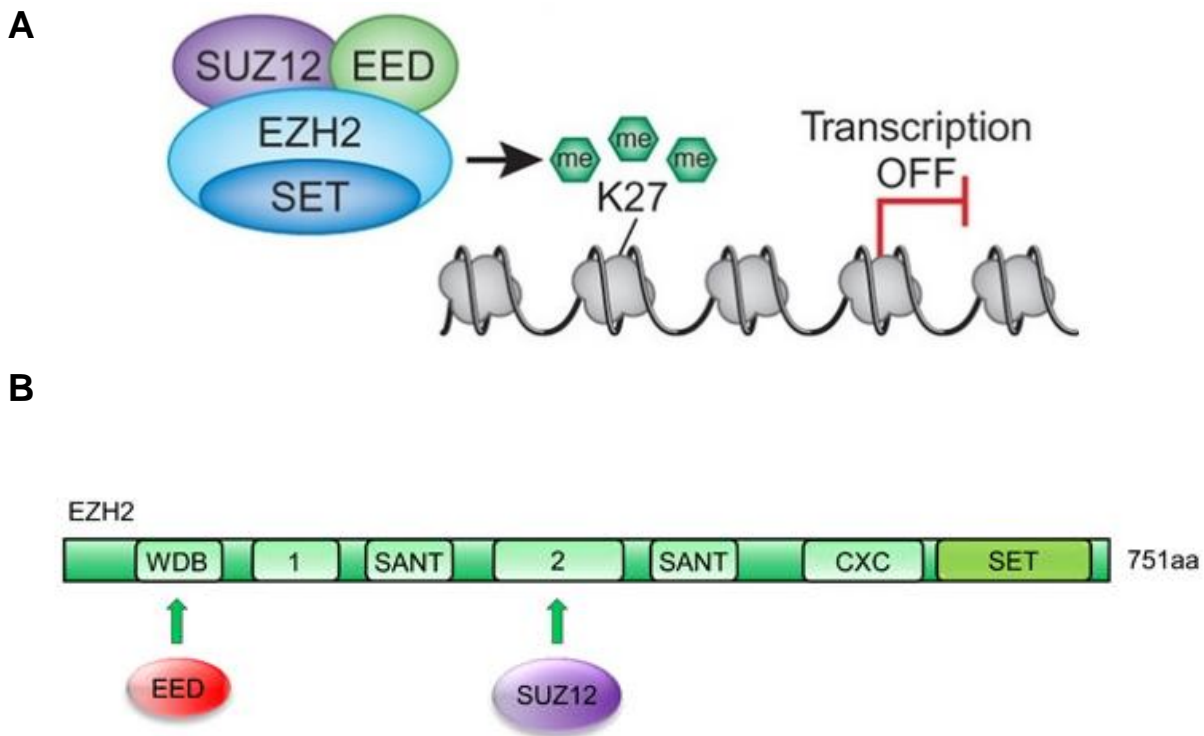
Figure 1-2: EZH2 is the core enzymatic component of PRC2 complex

(A) EZH2 interacts with other PRC2 proteins to mediate methylation of histone H3 at lysine 27 and silence gene expression. (B) Schematic illustration of EZH2 domains.

Fatty acid oxidation (FAO) is a catabolic process to degrade long-chain fatty acid with multiple steps to acetyl CoA and generating NADH and $FADH_2$ concomitantly. β-oxidation, the main form of FAO, primarily occurs in mitochondrion. During β-oxidation, long chain fatty acid must react with carnitine to form long chain acylcarnitine to cross mitochondrial membrane structure, and this is the rate limiting step of FAO, which is catalyzed by carnitine palmitoyltransferase 1 （CPT1)(*67, 68*). There are three types of CPT1- CPT1A or CPT1-liver is the main form in liver, kidney, lung, and ovary; CPT1B or CPT1-M is the dominant form in skeletal muscle, heart and

fat; CTP1C is limited to brain and testes (*69*, *70*). Following being shuttled into mitochondrial matrix, fatty acid was released by CPT2 from acylcarnitine to undergo FAO (*67*, *68*). Under physiological condition, only certain tissue types, such as liver, skeletal muscle, and heart, utilize FAO as a major energy source. It was thought that tumors seemed to rely on metabolizing glucose and glutamine (*71*, *72*), the importance of FAO in cancer has been undervalued until recent years. Tak Mak's group has found that FAO is responsible for cancer cell resistance to mTOR inhibition and to metabolic stress, such as glucose deprivation and hypoxia (*73*). Pilar *et al.* identified a certain subset of diffuse large B-cell lymphoma (DLBCL) that heavily relied on FAO for mitochondrial respiration and became more sensitive to FAO inhibition than other subsets (*74*). Ismael *et al*. characterized that pharmacological blockade of FAO by Etomoxir, which inhibits the activity of CPT1, sensitized leukemia cells to apoptosis induced by ABT-737. Since such suppression of FAO by Etomoxir in these leukemia cells did not affect ATP production, the result suggested a direct interaction between FAO pathway and mitochondrial pathway of apoptosis (*75*). In a more recent study, Wang *et al*. revealed that in colorectal cancer, FAO was necessary for the cancer cell survival under anoikis by producing more ATP and reducing NADPH to scavenge reactive oxygen species (ROS) and thereby promoted metastasis (*76*). In breast cancer, a metabolomic study has shown that TNBC patients have higher level fatty acids and carnitine metabolites in their plasma that suggests an altered FAO in TNBC (*77*). Similarly, Tianyi *et al.* discovered that FAO was required for self-renewal of breast cancer stem cells that accounts for breast cancer chemoresistance (*78*). Moreover, Camarda *et al*. revealed that MYC-high TNBC had stronger FAO than MYC-low TNBC and other receptor-positive breast cancer. Etomoxir treatment of MYC-high tumor allografts or patient derived xenografts (PDX), but not MYC-low tumors, significantly reduced tumor progression (*79*). Although these studies reveal an important role of

FAO in breast cancer, the underlying regulatory mechanism of FAO that can be exploited as effective treatments in heterogenous breast cancer, especially non-MYC-high tumors, remained to be elucidated.

1.3 Thesis goal and approach

This thesis project aims to (1) Determine whether and how PKM2 and EZH2 coordinately elicit a glycolysis-FAO switch in TNBC by Seahorse analyzer using various TNBC cell lines with genetically deletion of PKM2 and EZH2; (2) Determine whether combination of a clinically tested EZH2 inhibitor, GSK126 , and a clinically tested FAO inhibitor, Etomoxir, synergize in suppressing TNBC growth both *in vitro* (cell growth and colony formation assays) and *in vivo* (TNBC tumor xenograft mice); (3) Establish a role for EZH2 mediated metabolic regulation of dendritic cell (DC) generation by examining metabolic profiles in DCs treated with GSK126 using Seahorse analyzer.

1.4 Thesis layout

In Chapter 2, my findings reveal the role of PKM2-EZH2 in metabolic reprogramming of TNBC and demonstrate therapeutic efficacy of combining a clinically used EZH2 inhibitor with a clinically used FAO inhibitor for the treatment of TNBC vitro and in vivo. In Chapter 3, my pilot results reveal the role of EZH2 in metabolic regulation of in vitro generation of functional DCs.

CHAPTER 2.   THE ROLE OF PKM2-EZH2 IN METABOLIC REPROGRAMMING OF TRIPLE-NEGATIVE BREAST CANCER CELLS

2.1   Introduction

PKM2 is considered as a crucial glycolytic enzyme for maintaining glycolysis and cell proliferation in cancer cells. However, the oncogenic role of PKM2 in breast cancer is controversial. Liu *et al*. showed that PKM2 methylation by CARM1 was important for maintaining the glycolytic phenotype and reducing oxidative phosphorylation in breast cancer cells and this glycolytic phenotype was necessary for cell proliferation(*26*). On the contrary, Israelsen *et al*. demonstrated that PKM2 deletion did not inhibit or slow down tumorigenesis in a Brca1-driven TNBC mouse model(*27*). The later suggested that tumor cells may have a compensatory strategy to bypass the growth inhibition from deficient glycolysis. Although the replacement of total PKM by PKM2's alternative splicing counterpart PKM1 fully recovered glycolysis, the xenograft tumor growth of PKM1 rescued group was much slower than PKM2 rescued group, implicating a non-glycolytic function of PKM2(*16*). In addition, studies also revealed that PKM2 could act as a protein kinase and a co-activator to affect many cellular processes(*22*, *80*, *81*). Here, I will present PKM2 as a potential EZH2 interacting protein and a protein kinase of EZH2 that the two coordinately mediate of regulation of glycolysis and fatty acid oxidation in TNBC cells. By eliciting a metabolic switch to FAO through inhibition of EZH2, TNBC cells become more vulnerable to FAO inhibition.

2.2   Material and Methods

2.2.1   Cell lines

MDA-MB-231, BT549, MCF7 and HEK293T were purchase from ATCC. All of them were cultured with DMEM medium supplemented with 10% FBS, penicillin (50 U/mL), and streptomycin (50 U/mL).

2.2.2   Construction of CRSPR/Cas9 KO cells

To establish PKM2-KO cells, sgRNA designed by GPP sgRNA designer from Broad Institute was purchased from Cyagen Biosciences in an all-in-one vectors (including Cas9 and sgRNA). EZH2 sgRNA1 and sgRNA2 were purchased from ABM Inc. (K0012706, K0012707). For generation of PKM2-KO or EZH2-KO cell lines, cells were transfected with PKM2 sgRNA- or EZH2 sgRNA-contained all-in-one vectors. After transfection followed by 2.5 µg/mL puromycin selection for 3 days, the clones verified as positive PKM2-KO cells were collected as a cell pool.

2.2.3   Plasmid construct and lentiviral packaging

His-tagged PKM2 and GST-tagged EZH2 were cloned into pET empty vector. FLAG-tagged EZH2 and SLC16A9 was cloned into pCDH (a kind gift from Dr. Zhimin Lu at MD Anderson Cancer Center). shPKM2 and its control vector are also kind gifts from Dr. Zhimin Lu, the targeting sequence of shPKM2 is CATCTACCACTTGCAATTA, which is PKM2 exon 10 specific. shEZH2 was purchased from Sigma (TRCN0000293738). For lentiviral production, empty vectors and targeting vectors were co-transfected with psPAX2 and pMD2.G into HEK293T overnight by using PEI in the ratio of 4:1 to total plasmids amount. After replenishing medium next day, medium containing packaged virus was collected twice at 48 h and 72 h respectively after transfection. Then, medium was filtered through 0.4µm filter and concentrated by adding Lenti-X concentrator (Takara, 631232) following manufacturer's instruction. Next,

subconfluent targeted cells were infected by harvested lentivirus with 5µg/mL polybrene. Lentivirus transformed cells were selected in 2.5µg/mL puromycin for 1 week and maintained in 0.5µg/mL puromycin.

2.2.4 GST pulldown

His-PKM2 and GST-EZH2 with full length or truncated forms were over-expressed in E. coli BL21 (DE3, New England BioLabs) and induced by 0.4 mM IPTG (Sigma) for three hours at 37 °C in LB medium when the absorbance value of medium at 600nM reached at around 0.5-0.7. Bacterial were then lysed, sonicated and supernatant was collected by centrifuge. His-PKM2 was affinity purified by using a His GraviTrap column (GE Healthcare, 11-0036-89). GST-tagged various EZH2 forms were purified by MagneGST Protein Purification System (Promega, V8600). After 3 h co-incubation of purified proteins at room temperature, the proteins and beads complex were washed three times with pull-down buffer and then prepared for immunoblotting.

2.2.5 Immunoprecipitation and immunoblot

Cells were lysed in 1X lysis buffer (CST, 9803) with supplements of protease inhibitor cocktail (GenDEPOT, P3100) and phosphatase inhibitor cocktail (BOXTER, AR1183). Lysate were then sonicated and pelleted. Supernatant was immunoprecipitated overnight by targeting antibodies or an isotype control antibody plus Protein A/G Plus-Agarose (Santa Cruz, sc-2003). Precipitated samples were washed by lysis buffer for three times the next day and boiled in 1X Loading buffer for 5 min. After placing on ice for 5 min, samples were stored in -80 °C or loaded into SDS-PAGE and immunoblotted by interested antibodies with dilutions as following: PKM2 mAb (CST, 4053) at 1:3000, PKM1 mAb (CST, 7067) at 1:2000, EZH2 mAb (CST, 5246) at 1:2000, HA-Tag mAb (CST, 3724) at 1:3000, Flag-Tag mAb (Sigma, F3165) at 1:3000, Phospho-SMAD2 mAb (CST, 3108) at 1:1000, Histone H3 mAb (CST, 4499) at 1:3000, Tri-Methyl-Histone H3 (Lys27) mAb

(CST, 9733) at 1:1000, GST-Tag mAb (CST, 2625) at 1:3000, ACTIN mAb (Sigma, A5441) at 1:5000, SUZ12 mAb (CST, 3737), HIS-Tag mAb (CST, 12698) at 1:3000, Phospho-Ser/Thr mAb (BD, 612548) at 1:1000, pThr-Pro mAb (CST, 9391) at 1:1000, TUBLIN mAb (Active Motif, 39528) at 1:3000.

2.2.6　Real-time PCR

Total RNA was extracted from cell with the RNA extraction kit (Zymo Research, R1057). Then RNA was reverse transcribed to cDNA by using SuperScript III kit (Invitrogen, 18080051). Real-time PCR was performed by using FastStart Essential DNA Green Master according to manufacturers' instruction (Roche, 6402712001). For Human Fatty Acid Metabolism PCR array (Qiagen, PAHS-007ZD-6), RT² First Strand Kit (Qiagen, 330401) and RT² SYBR Green qPCR Mastermix (Qiagen, 330501) were used for reverse transcription and real time qPCR accordingly. The RNA amount of gene of interest (GOI) was calculated with 2 to the power of ΔCt (Ct_{GOI}-$Ct_{\beta\text{-}ACTIN}$). The relative of fold change was calculated with 2 to the power of $\Delta\Delta$Ct. Primers were listed as following: PKM2 forward primer: CATTACCAGCGACCCCACAGAAG, PKM2 reverse primer: GAGGACGATTATGGCCCCACTGC, SLC16A9 forward primer: GATGCCTTTGGTGAAGGAAA, SLC16A9 reverse primer: CACAGAGACTGCAGACAGGACT, ACTIN forward primer: GTGGGCATGGGTCAGAAG, ACTIN reverse primer: TCCATCACGATGCCAGTG, SLC16A1 forward primer: TTTCTTTGCGGCTTCCGTTG, SLC16A1 reverse primer: GGACAGGACAGCATTCCACA, SLC16A3 forward primer: TGATTTTGCTGCTGGGCAAC, SLC16A3 reverse primer: TCCCCGTTTTTCTCAGGCTC, SLC37A4 forward primer: AGTACCTGTCTTTGCTGCCC, SLC37A4 reverse primer: GGATGGTTGCCAGGATAGGG, SLC27A2 forward primer: TGCTGCACTACTGATTGGCA, SLC27A2 reverse primer: TTTCCCAGTGCCAGTCTCAC,

SLC37A1 forward primer: GAACAGGAAGTCTGGGTCCG, SLC37A1 reverse primer: CCCAATGATGCCACTGAGGT.

2.2.7   Cell proliferation assay

MTT solution was prepared in PBS (5mg/mL). 5000 MDA-MB-231 cells were seeded in 96 well plates per well. After three days drug treatment at indicated concentration, one tenth MTT of the volume of medium was added into each well. After 2 h-3 h incubation in cell culture incubator, medium was removed and 100μL DMSO was added into each well. Absorbance value at 590nm was read after MTT was well dissolved in DMSO.

CCK8 solution was purchased from Dojindo Molecular Technologies, Inc. (CK04-11). 1500 MDA-MB-231 cells and 2500 BT549 cells were seeded per well in 96 well plates. After 6 days drug treatment at indicated concentration, one tenth CCK8 of the volume of medium in each well was added into each well. After 2 h-3 h incubation in cell culture incubator, absorbance value at 450nm was read after shaking the plates on an orbiter shaker for 15 min.

SRB assay was perform according to the description of a previous study(*82*). Briefly, cells in 96 well plates were fixed with 100μL 10% Trichloroacetic acid for 1h at 4°C. Then, cells were washed thoroughly by tap water for 3-4 times and air dried. Cells were stained with 0.06% SRB for 30 min and washed by 1% acetic acid thoroughly for 3-4 times. After cells were air dried, 100μL of 10mM Tris base solution (pH 10.5) was added into each well. Absorbance value at 530nM was read after SRB was completely dissolved in Tris base solution.

2.2.8 Colony formation assay

500 MDA-MB-231 cells and 2000 BT549 cells were seeded per well in 24 well plates. After 10 days drug treatment at indicated concentration, cells were fixed by fixation solution Acetic acid/methanol 1:7 (vol/vol) for 5m. Cells were then stained by 0.5% crystal violet for 30m and washed by tap water.

2.2.9 Seahorse Extracellular Flux analysis

15000 MDA-MB-231 cells were seeded per well in XF96 assay plates (Agilent, 101085-004). Cells were washed two time with assay media, Seahorse XF DMEM medium pH 7.4 (Agilent, 103575-100) supplemented with 25mM Glucose, 4mM Glutamine, 1mM Pyruvate and kept in assay media. For the measurement of endogenous substrates, 15 min before assay, Etomoxir was manually added into related wells at a final concentration of 50μM, UK5099 was added at a final concentration of 2 μM and BPTES was added at a final concentration of 3 μM. During the assay, oxygen consumption (OCR) was measured at basal status and after Mito Stress Test compounds treatment (4μM oligomycin, 2μM FCCP and 2μM rotenone and antimycin A was injected into designed wells by the machine at indicated time points). For exogenous FAO measurement, cells were seeded in XF96 assay plate and were starved for one day in the substrate-limited medium (Seahorse XF DMEM medium pH 7.4 supplemented with 0.5 mM glucose, 1 mM GlutaMAX, 0.5 mM carnitine). On the assay day, cells were washed two times by the assay media (Seahorse XF DMEM medium pH 7.4 supplemented with 2.5 mM glucose, 0.5 mM carnitine) and kept in assay media. Right before the following mito stress test assay, 30 μL XF Palmitate-BSA FAO Substrate or BSA (Agilent, 102720-100) is added to the appropriate well. Basal respiration was calculated by the OCR at basal status minus the OCR after the addition of rotenone and antimycin A. Maximal respiration was calculated by the OCR after FCCP treatment subtracts the OCR after the addition

of rotenone and antimycin A. For glycolysis measurement, proton efflux rate (PER) was measured under both basal condition and in response to 0.5μM rotenone and antimycin A, and 50mM 2-DG.

2.2.10 Measurement of intracellular Carnitine, and ATP levels

Intracellular carnitine content was measured by L-Carnitine Assay Kit from Sigma (MAK063-1KT). ATP amount was measured by ATP Detection Assay Kit – Luminescence from Cayman (700410).

2.2.11 Immunohistochemistry staining

Sections of formalin fixed tissue microarray slides from breast cancer patients (BRC1021, Pantomics) were deparaffinized and rehydrated in various xylene and ethanol solution. After antigen retrieval by heating, sections were blocked with 5% BSA and then incubated overnight at 4°C with indicated primary antibodies. Next, after appropriate secondary antibody was applied to the section for 1h at room temperature, washed and visualized with DAB chromogen kit (BioCare medical), slides were counterstained with hematoxylin. Images were taken by Olympus BX53 Upright Microscope.

2.2.12 Xenograft model

2×10^6 luciferase expressing MDA-MB-231 (GeneCopoeia, #SL018) was orthotopically implanted in the 4th mammary gland on the right side of 6-8 weeks female SCID mice (Roswell Park Cancer Institute). After 2 to 3 weeks growth, mice were grouped according to the bioluminescent intensity. Mice were daily received 50 mg/kg GSK126 (Cayman, 15415), 40 mg/kg Etomoxir (Selleckchem, S8244) or vehicle by i.p. injection for 2 weeks. Tumor growth was determined by bioluminescent signal after i.p. injection of luciferin (150mg/kg). After euthanizing the mice, tumors were collected for further evaluation. All animal experiments were conducted

with approval of the Institutional Animal Care and Use Committee (IACUC) at Roswell Park Cancer Institute.

2.2.13 Statistical analysis

Each experiment was conducted independently for at least three times. The animal cohorts for experiments are with same strain, sex, size, and allocated to different experimental groups by randomization. Sample size was chosen based on power analysis (desired power=80% and significance P<0.05). Differences between individual groups were analyzed by Student's t test or by one-way ANOVA test for multiple group analysis. Experimental models were randomly distributed over treatment groups. If not otherwise noted, no methods were used to determine whether the data met assumptions of the statistical approach; no inclusion/exclusion criteria/cases were applied. All analyses were carried out using Microsoft Excel or GraphPad Prism 7 and presented as means± the standard deviation of the mean (SD). P value of 0.05 or lower were considered statistically significant for all experiments. The statistical parameters can be found in the figure legends.

2.3   Results

Although it has been widely shown that PKM2 ablation results in increased mitochondrial respiration, which mitochondrial fuel resource utilization is augmented after abolishing PKM2 is not clear. To answer this question in TNBC, I first stably knocked down PKM2 expression (shPKM2) in MDA-MB-231 cells by using short hairpin RNA. Then, I used Seahorse XF analyzer to measure the oxygen consumption rate (OCR) changes in response to each of three major mitochondrial fuels, pyruvate, glutamine, or fatty acid, by adding their oxidation inhibitor, respectively, UK5099 (inhibitor of pyruvate oxidation), BPTES (inhibitor of glutamine oxidation),

and Etomoxir (inhibitor of fatty acid oxidation, FAO). OCR due to enhanced FAO was increased upon PKM2 knockdown and this increase was not related to pyruvate and glutamine mediated oxidation (Figure 2-1 A, 2-1 B and 2-1 C). The ability to utilize exogenous long chain fatty acid (palmitic acid, palm) for respiration was also enhanced upon PKM2 knockdown in MDA-MB-231 cells (Figure 2-1 A). Moreover, there was a decrease of glycolysis in PKM2 knockdown MDA-MB-231 cell as shown by reduced glycolytic proton efflux rate (GlycoPER) (Figure 2-1 D). Furthermore, using qPCR gene expression arrays that consisted around 100 fatty acid metabolism related genes, the data concordantly revealed that expression of the genes involved in FAO and lipid import, including ACADL, ACADS, ACOX2, CPT1C, PRKAA2, FABP5, FABP6, and LPL, was significantly upregulated in PKM2 knockdown cells (Figure 2-1 E). By staining neutral lipids with Oil-O-Red, I found that there were more lipids in shPKM2 cells which implicates a more lipid uptake from medium echoing the upregulation of genes involved in lipid import in the PCR array data (Figure 2-1 F). These results implicate that inhibition of PKM2 elicits a metabolic switch from utilizing glycolysis to FAO in TNBC cells. As it has been revealed that FAO is important for generating ATP(*72*, *83*), I next used Etomoxir to determine the contribution of FAO to ATP production in MDA-MB-231 shPKM2 cells. Compared with the control cells, treatment of Etomoxir caused a significant reduction of ATP in shPKM2 cells (Figure 2-1 G). These data suggest that PKM2 knockdown TNBC cells may rely more on FAO for cell growth. To test this hypothesis, I measured the cell growth of shPKM2 MDA-MB-231 cells by MTT with various concentrations of Etomoxir treatment. shPKM2 and the control MDA-MB-231 cells showed similar cell growth rate under normal cell culture condition; however, shPKM2 cells were significantly sensitive to Etomoxir induced- cell growth inhibition and Etomoxir induced- colony formation inhibition (Figure 2-1 H, Figure 2-1 I). To further validate the results, I generated PKM2

knockout (KO) MDA-MB-231 cells by transfection of a CRISPR/Cas9 plasmid that specifically targets PKM2 exon 10, followed by antibiotic selection of the cell pool that had a loss of PKM2 expression with little compensatory PKM1 induction. Similar to knockdown of PKM2, knockout of PKM2 alone did not inhibit cell growth but sensitized cells to Etomoxir treatment (Figure 2-1 G and 2-1 K). Together, these data suggest that inhibition of PKM2 elicits a metabolic switch from utilizing glycolysis to FAO that would likely sustain TNBC cells in the absence of PKM2.
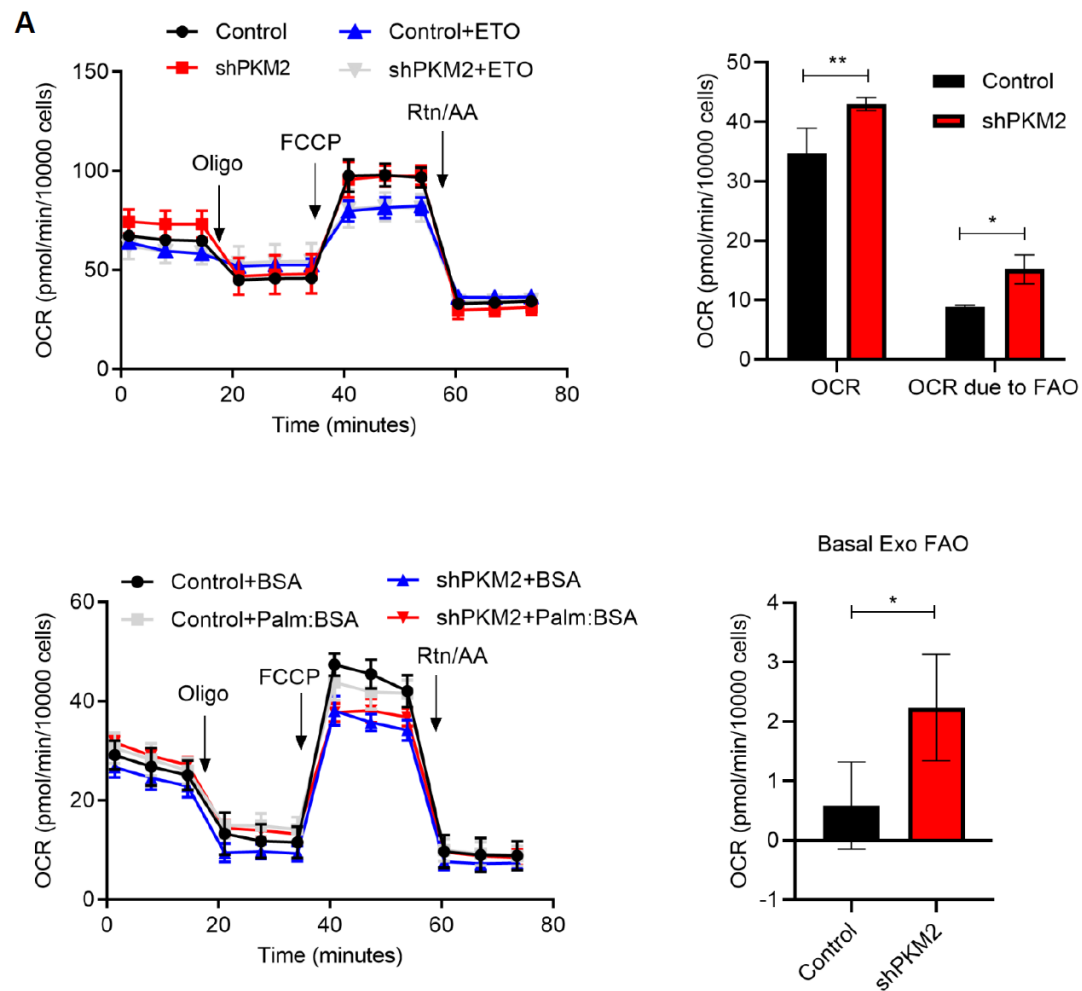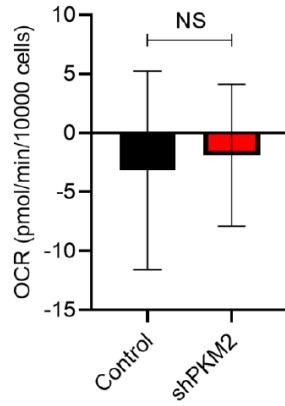
Figure 2-1: PKM2 ablation leads to a metabolic switch from glycolysis to fatty acid oxidation in TNBC cells
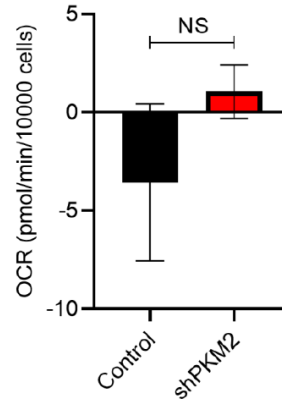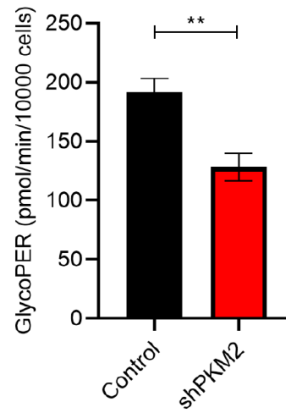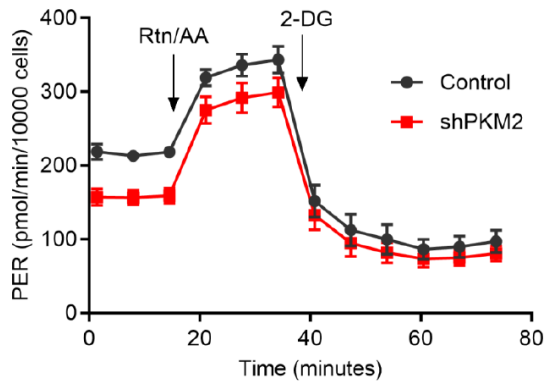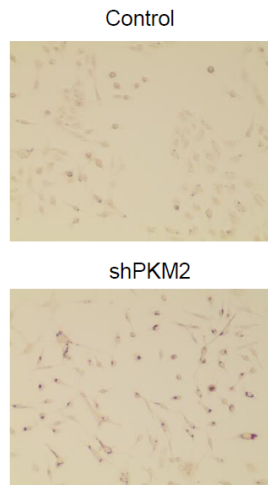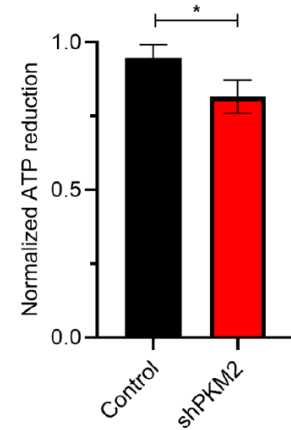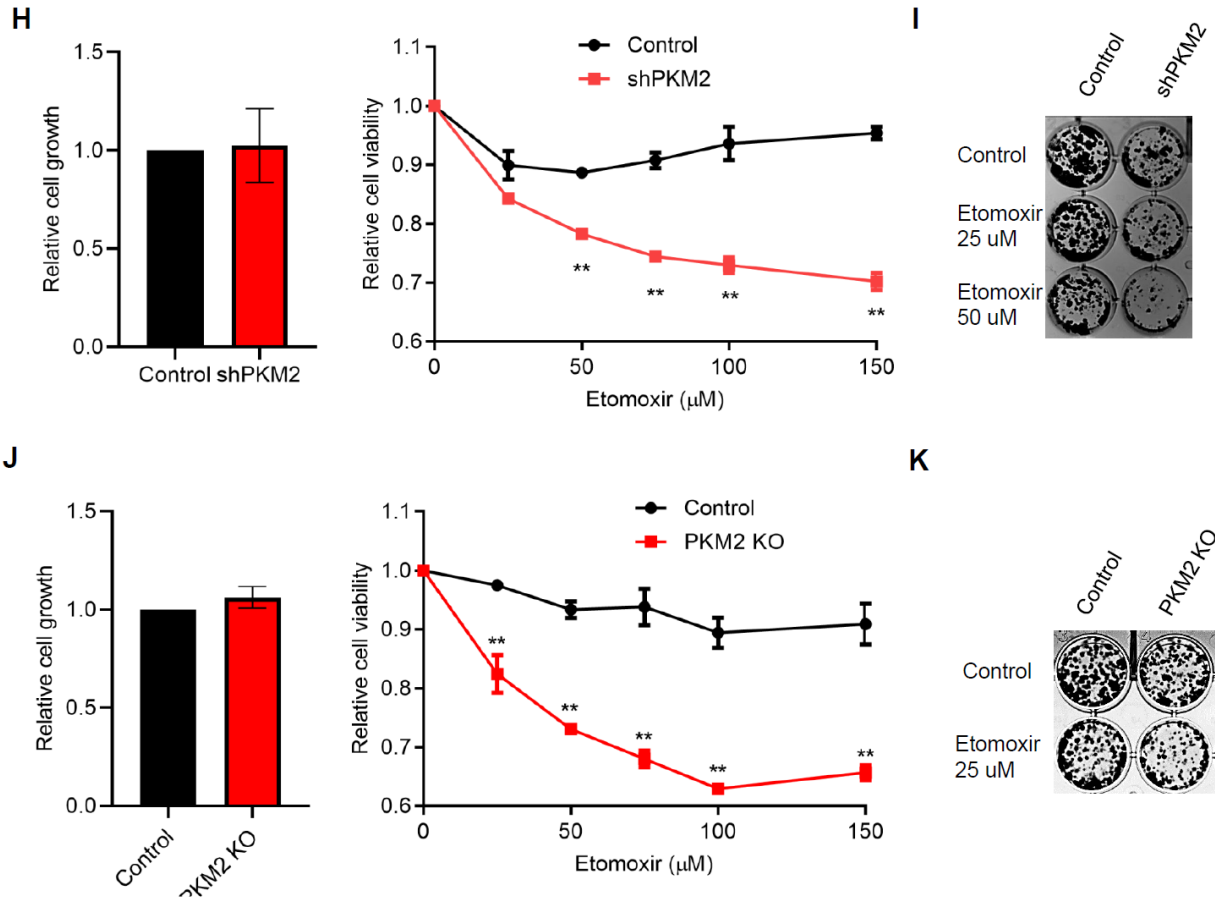
Figure 2-1 continued
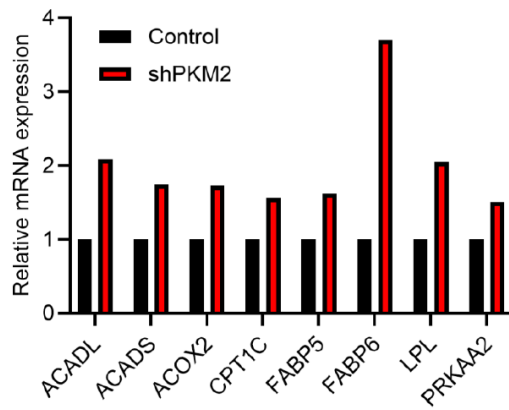
Figure 2-1 continued

(A) Endogenous and Exogenous fatty acid oxidation in MDA-MB-231 cells. (B) Mitochondrial respiration due to utilization of pyruvate. (C) Mitochondrial respiration due to utilization of glutamine. (D) Glycolysis measurement in MDA-MB-231 cells. (E) PCR array result of most upregulated fatty acid metabolism related genes in MDA-MB-231 shPKM2 cells. (F) Neutral lipid staining by Oil-O-Red in MDA-MB-231 shPKM2 cells. (G) ATP measurement after Etomoxir (50 μM) treatment for 1d in MDA-MB-231 shPKM2 cells. (H) Cell viability measurement by MTT after Etomoxir treatment at indicated concentration for 3d in MDA-MB-231 control or shPKM2 cells. (I) Colony formation assay of MDA-MB-231 control or shPKM2 treated with indicated concentration of Etomoxir. (J) Cell viability measurement by MTT after Etomoxir treatment at indicated concentration for 3d in MDA-MB-231 control or PKM2 KO cells. (K) Colony formation assay of MDA-MB-231 control or PKM2 KO treated with indicated concentration of Etomoxir. Asterisk indicates $P<0.05$; double asterisks indicate $P<0.01$. Error bars denote ±SD.

To explore which cellular processes PKM2 has an effect on in TNBC, we first did a liquid

chromatography tandem mass spectrometry (LC-MS/MS) after immunoprecipitating PKM2 from

MDA-MB-231 cells to identify its binding partners. Among a total of 961 detected proteins, there are a lot of chromosome associated proteins. Besides the reported histone H3, all other nucleosome histones, H1, H2A, H2B, H4, were also co-immunoprecipitated by PKM2, suggesting a possible chromatin association of PKM2. Intriguingly, two PRC2 complex components, EZH2 and SUZ12, were also discovered. As EZH2 is crucial for breast cancer progression, we would like to address the importance of the interaction of PKM2 and EZH2 in TNBC. To confirm our LC-MS/MS result, a reciprocal co-immunoprecipitation in HEK293T cells was conducted and the result showed that the exogenously expressed PKM2 and EZH2 interacted with each other (Figure 2-2 A). Next, by purifying PKM2 and EZH2 from transformed E. Coli followed by a co-immunoprecipitation, the direct physical interaction between PKM2 and EZH2 was proved (Figure 2-2 B). To narrow down which domain of EZH2 binds to PKM2, EZH2 was truncated into three different fragments and the CXC domain (aa523-aa509) was found to be the predominant part of EZH2 to associate with PKM2 (Figure 2-2 C), suggesting a possible role of PKM2 in regulating the histone methyltransferase activity of EZH2 via interacting with CXC. To determine whether there is an interaction between PKM2 and EZH2 in TNBC, we performed an endogenous reciprocal co-immunoprecipitation in MDA-MB-231 cells and validated the association between PKM2 and EZH2 in TNBC (Figure 2-2 D). Interestingly, this interaction did not exist in non-invasive luminal breast cancer cells, MCF7 (Figure 2-2 E). As MCF7 is more like epithelial cell-like phenotype and MDA-MB-231 exhibits more mesenchymal-cell like feature, I explored the effect of an epithelial mesenchymal transition (EMT) inducer, TGF-β1, on the interaction between PKM2 and EZH2. TGF-β1 treatment enhanced the interaction between PKM2 and EZH2 and this interaction was mainly taken place in the nucleus (Figure 2-2 F, G and H). The above results suggest that PKM2

can interact with EZH2 in TNBC cells and this interaction may be affected by oncogenic stimuli that promote EMT and invasive traits of TNBC, such as TGF-β1.
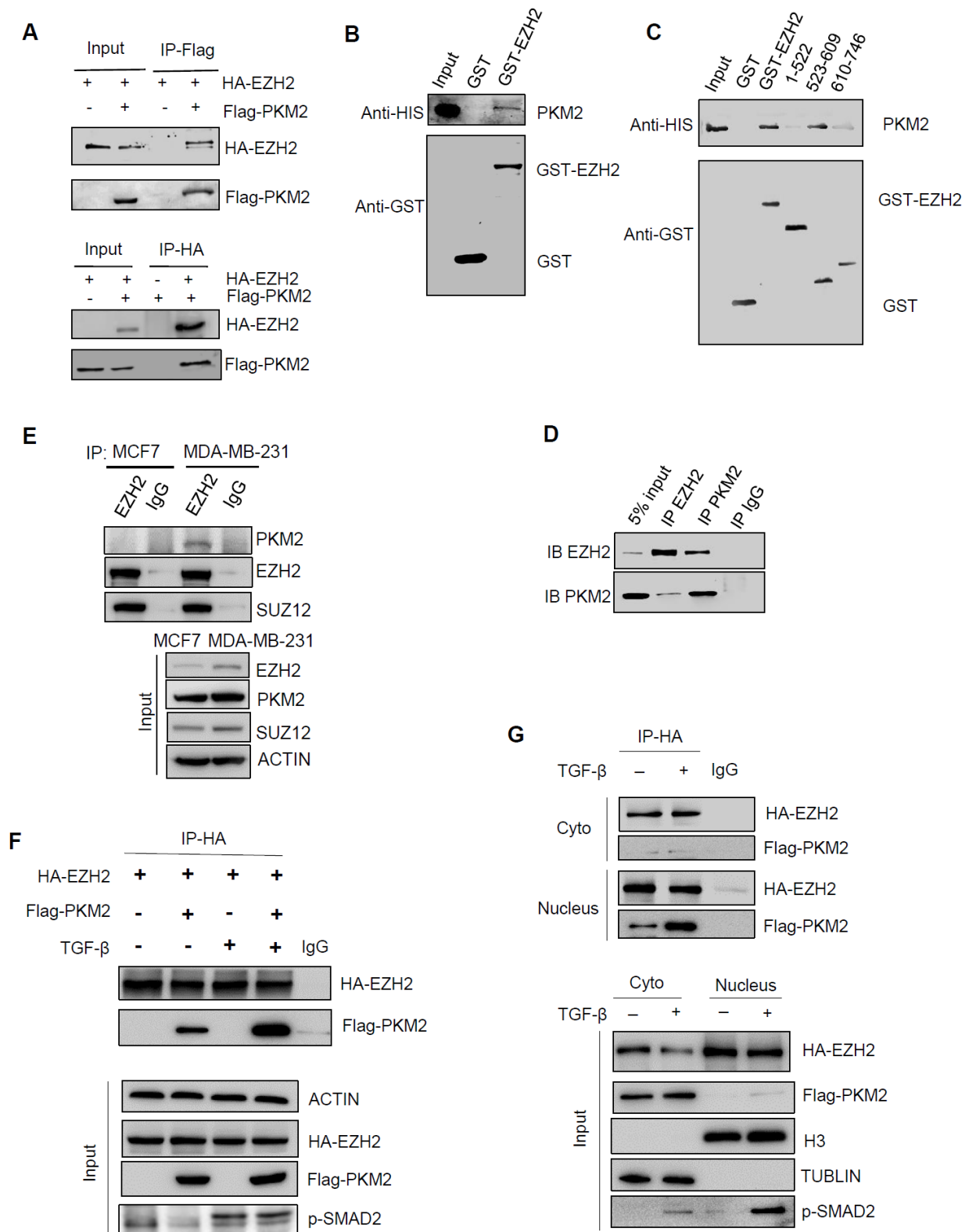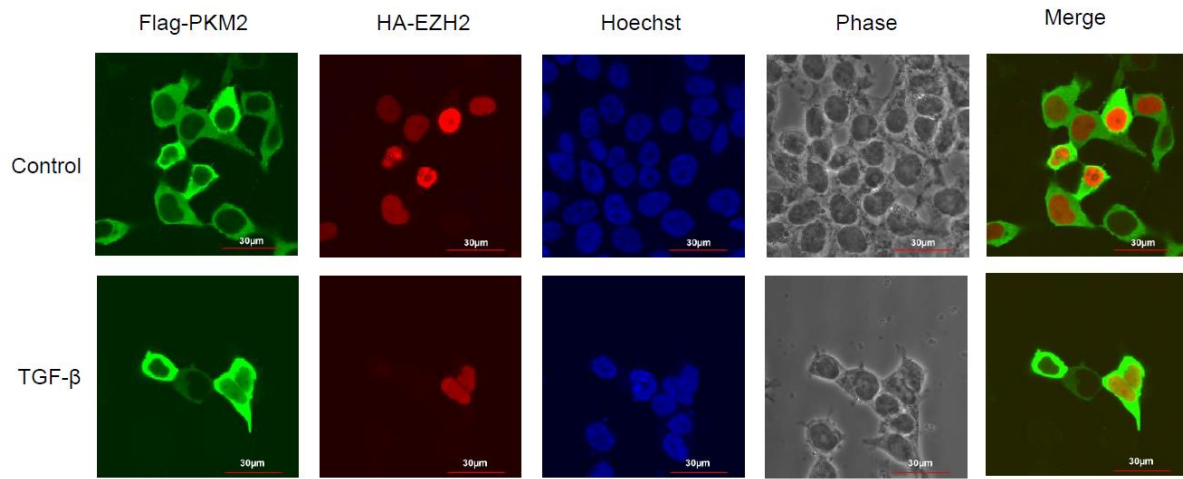
Figure 2-2: PKM2 directly interacts with EZH2 and the interaction is enhanced by TGF-β1

Figure 2-2 continued

H

(A) Reciprocal co-immunoprecipitation of exogenously expressed PKM2 and EZH2 in HEK293T cells. (B-C) GST pulldown of full-length of EZH2 (B) and truncated EZH2 (C) with PKM2. (D) Reciprocal co-immunoprecipitation of endogenous PKM2 and EZH2 in MDA-MB-231 cells. (E) The interaction between EZH2 and PKM2 in MDA-MB-231 cells and MCF-7 cells. (F-G) The interaction between exogenously expressed EZH2 and PKM2 in whole lysate (F) or subcellular fraction (G) of HEK293T cells with TGF-β1 (20ng/mL) treatment for 24h. (H) Representative Immunofluorescence images of the colocalization 0f exogenous FLAG-PKM2 and HA-EZH2 in HEK293T cells with or without TGF-β1 (20ng/mL for 2h).

EZH2 mediates trimethylation of H3K27 to silence target gene expression. The CXC domain adjacent to the catalytic SET domain of EZH2 is suggested to mediate binding of the substrate nucleosome and is required for histone methyltransferase activity. Since PKM2 was directly interacted with EZH2 through EZH2 523-609 in the CXC domain, I next studied whether PKM2 interaction with EZH2 would affect EZH2 methyltransferase activity. I found that knock-down of PKM2 led to significantly reduced H3K27Me3 level in both MDA-MB-231 and BT549 cells (Figure 2-3 A). A similar result was shown in PKM2 KO MDA-MB-231 cells (Figure 2-3 B). These data suggest that PKM2 expression is important for maintaining H3K27Me3 level in TNBC cells. It has been shown that PKM2 can act as a protein kinase and that phosphorylation of EZH2

at certain sites is required for its histone methyltransferase activity (*22*, *24*, *36*). We therefore started to interrogate whether PKM2 mediated phosphorylation of EZH2. A mass spectrometry phosphorylation comparison analysis was first performed in PKM2 KD (siPKM2) cells compared with the control MDA-MB-231 cells, and in Flag-PKM2 overexpression cells compared with the control MCF-12A cells. The result of these two comparisons revealed that PKM2 expression was important to the phosphorylation of EZH2 at the Thr367 (data not shown). To confirm this result, wild-type PKM2 or PKM2 kinase dead mutant (K367M) was overexpressed in MCF12A cells and endogenous EZH2 was then immunoprecipitated. Because there was no commercially available antibody for the EZH2 T367 phosphorylation, a pan-phospho-Ser/Thr antibody was used to detect the overall phosphorylation of EZH2. Overexpression of PKM2 enhanced the phosphorylation of EZH2 which was abolished after treating the sample with phosphatase. However, overexpression of the kinase dead mutant PKM2 (K367M) did not affect the phosphorylation of EZH2 (Figure 2-3 C). Same result was also shown with exogenously expressed EZH2 (Figure 2-3 D). Furthermore, in PKM2 KO MDA-MB-231 cells, EZH2 phosphorylation was robustly decreased using a more specific antibody that only detected the signal of a phosphorylated Threonine followed by a Proline, mimicking the motif that Thr367 is located in EZH2. Notably, the interaction between PKM2 and EZH2 was abolished in PKM2 KO MDA-MB-231 cells (Figure 2-3 E). As Thr367 is located in the long non-coding RNA (lnc-RNA) binding domain of EZH2, and EZH2 bound lncRNA has been shown to be critical for EZH2-DNA binding and target selection (*41*, *84*). Therefore, an EZH2-lnc-RNA RIP-PCR analysis was carried out. Four lncRNAs were identified, and two of them, ZFAS1 and TUG-1, were re-confirmed by real-time qRT-PCR (Figure 2-3 F). Together, these results suggest that PKM2 is crucial for maintaining H3K27Me3 level through phosphorylation of EZH2 at Thr367 that may impact its lncRNA binding ability.
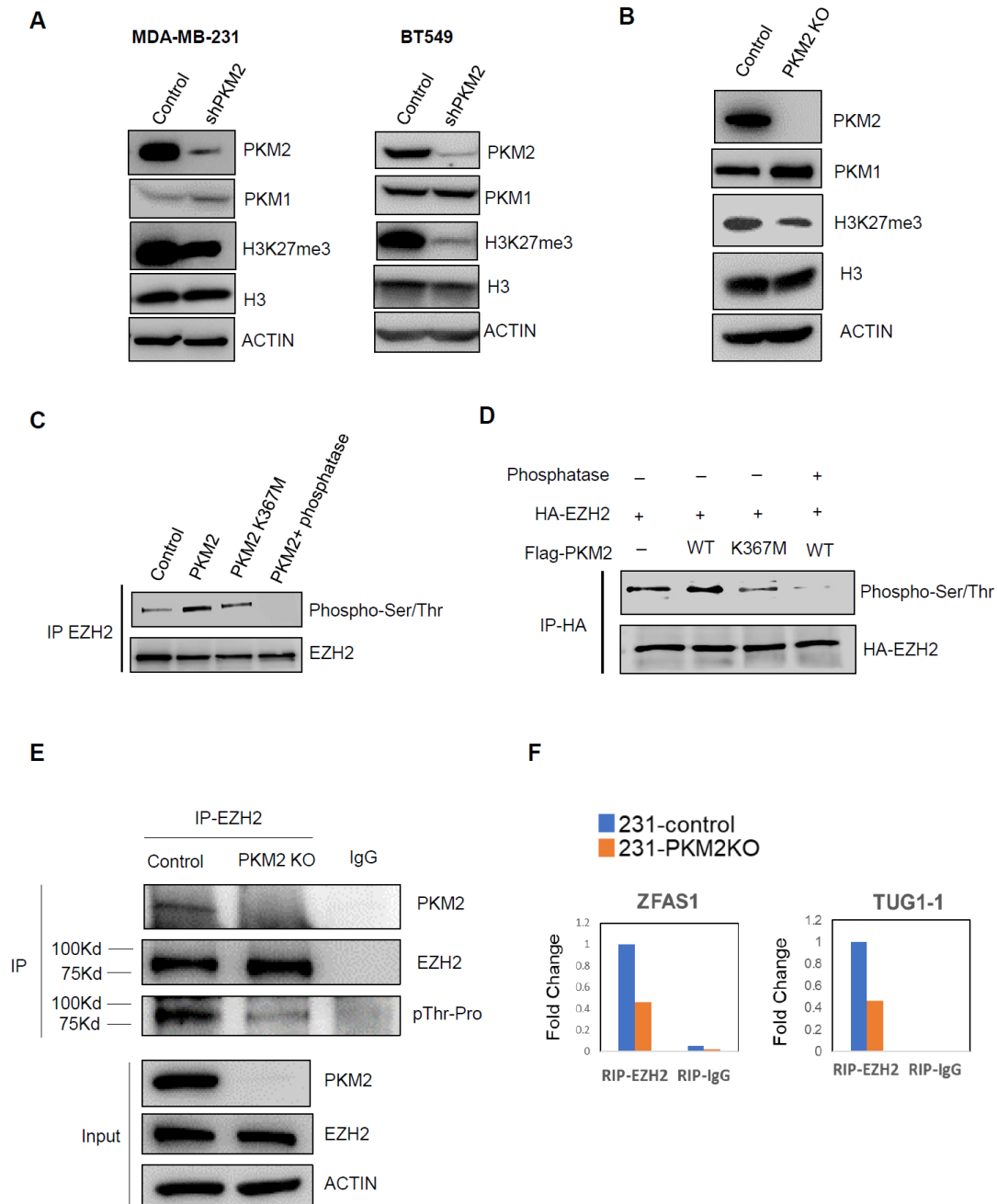
Figure 2-3: PKM2 is critical for H3K27Me3, potentially by mediating EZH2 phosphorylation and its interaction to specific lncRNAs

(A) H3K27Me3 level in MDA-MB-231 and BT549 after PKM2 KD. (B) H3K27Me3 measurement in MDA-MB-231 PKM2 KO cells. (C-D) Endogenous EZH2 (C) and exogenous EZH2 (D) phosphorylation in MCF12A after PKM2 WT or its kinase dead mutant (K367M) overexpression. (E) Endogenous EZH2 phosphorylation in MDA-MB-231 PKM2 KO cells. (F) The binding of lncRNAs to EZH2 after PKM2 KO in MDA-MB-231.

To determine the functional role of PKM2 mediated-regulation of H3K27Me3, a genome-wide chromatin immunoprecipitation sequencing (ChIP-seq) analysis was conducted via immunoprecipitating H3K27Me3. Compared between the control cells and the PKM2 KO cells, H3K27Me3 occupancy was most discriminated in a cohort of genes involved in metabolism related solute carrier family proteins. With a PANTHER Biological Process analysis, it was noted that the majority of genes that H3K27Me3 was differentially located in these two groups is involved in metabolism related pathways, including the solute carrier (SLC) family (Figure 2-4 A). Most of SLC family members is located in the cell membrane and are responsible for exchanging nutrients and ions between cells and their microenvironment. It has been shown that expression of many SLC family genes in cancer is dysregulated. To determine which SLC family gene was most significantly affected by PKM2 expression, a realtime qPCR screening was performed on the ChIP-seq targets. SLC16A9 was most significantly upregulated upon knockdown of PKM2 (Figure 2-4 B). Consistently, expression level of SLC16A9 was significantly upregulated upon knockout/knockdown of PKM2 (Figure 2-4 C-D) and also reduced by knockout of EZH2 (Figure 2-4 E). Together, these data suggest that PKM2 maintains EZH2 activity to silence gene expression involved in FAO, including SLC16A9 that mediates intracellular Carnitine transport for FAO.
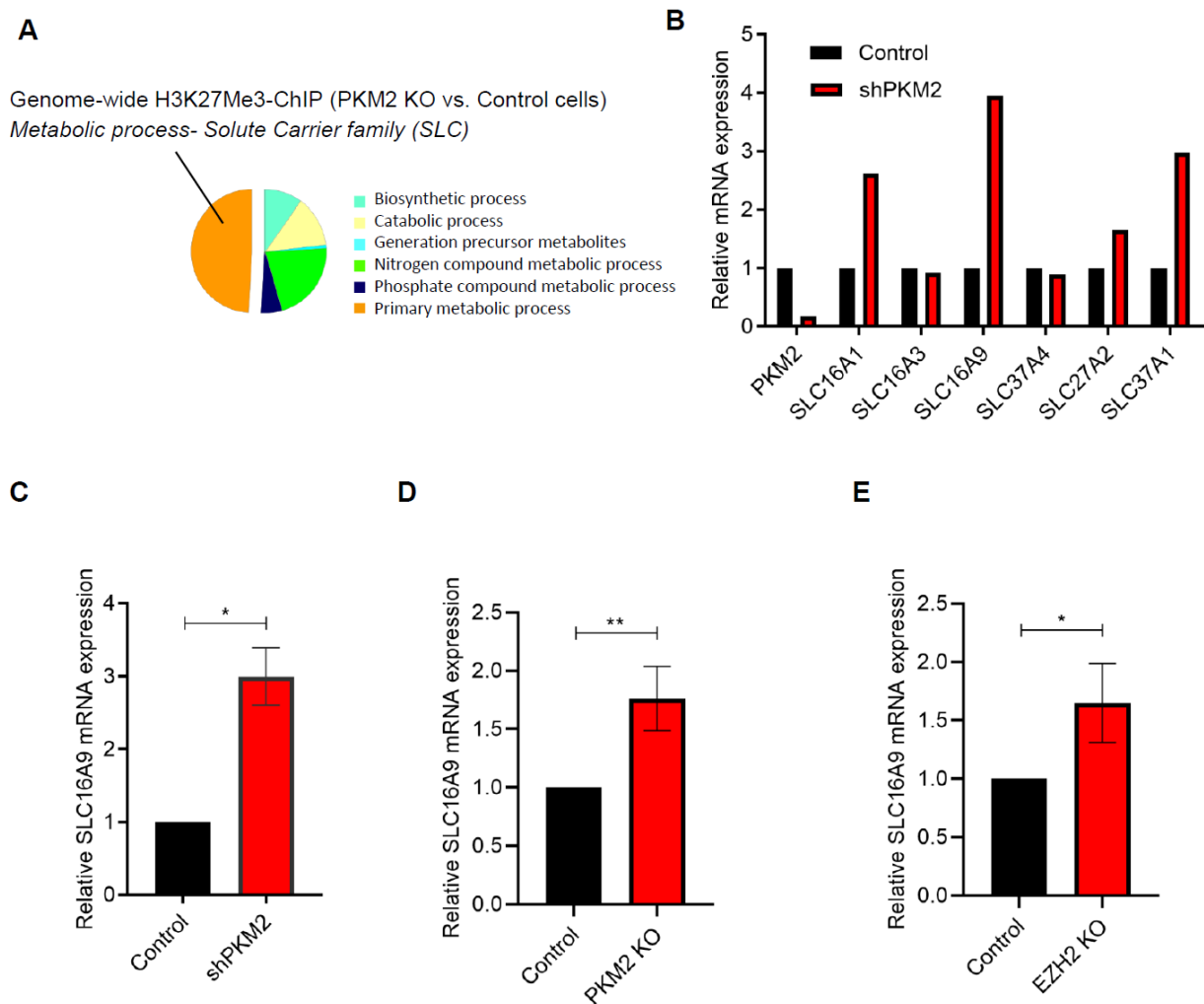
Figure 2-4: PKM2/EZH2 inhibit gene expression of metabolite-solute carrier family proteins, SLC16A9

(A) Panther Biological Process analysis of the genes with different abundance of H3K27Me3 after PKM2 KO in MDA-MB-231 cells. (B) qRT-PCR screening of SLC family genes identified in (A) in MDA-MB-231 shPKM2 cells. (C-E) Relative SLC16A9 expression in MDA-MB-231 shPKM2 (C), PKM2 KO (D), and EZH2 KO cells (E). Asterisk indicates $P<0.05$; double asterisks indicate $P<0.01$. Error bars denote ±SD.

Concordant to the data in Figure 2-4, we showed that knockdown of PKM2 that increased SLC16A9 expression was able to significantly enhance intracellular Carnitine level in both TNBC cell lines, MDA-MB-231 and BT549 (Figure 2-5 A). Intracellular Carnitine was consistently upregulated by knockout of PKM2 or EZH2 (Figure 2-5 B-C). As a result of increased intracellular

Carnitine, knockout or knockdown of EZH2 led to markedly enhanced basal and maximal FAO (Figure 2-5 D-G), which could be recapitulated upon inhibition of EZH2 by a small molecule inhibitor, GSK126 (Figure 2-5 J-K). Moreover, the ability of utilize exogenous long chain fatty acid (palmitic acid, palm) for mitochondrial respiration was also enhanced upon knockdown of EZH2 (Figure 2-5 H-I). In summary, these findings suggest that inhibition of PKM2/EZH2 led to increased SLC16A9 and intracellular Carnitine that can activate a metabolic switch to FAO in TNBC cells.
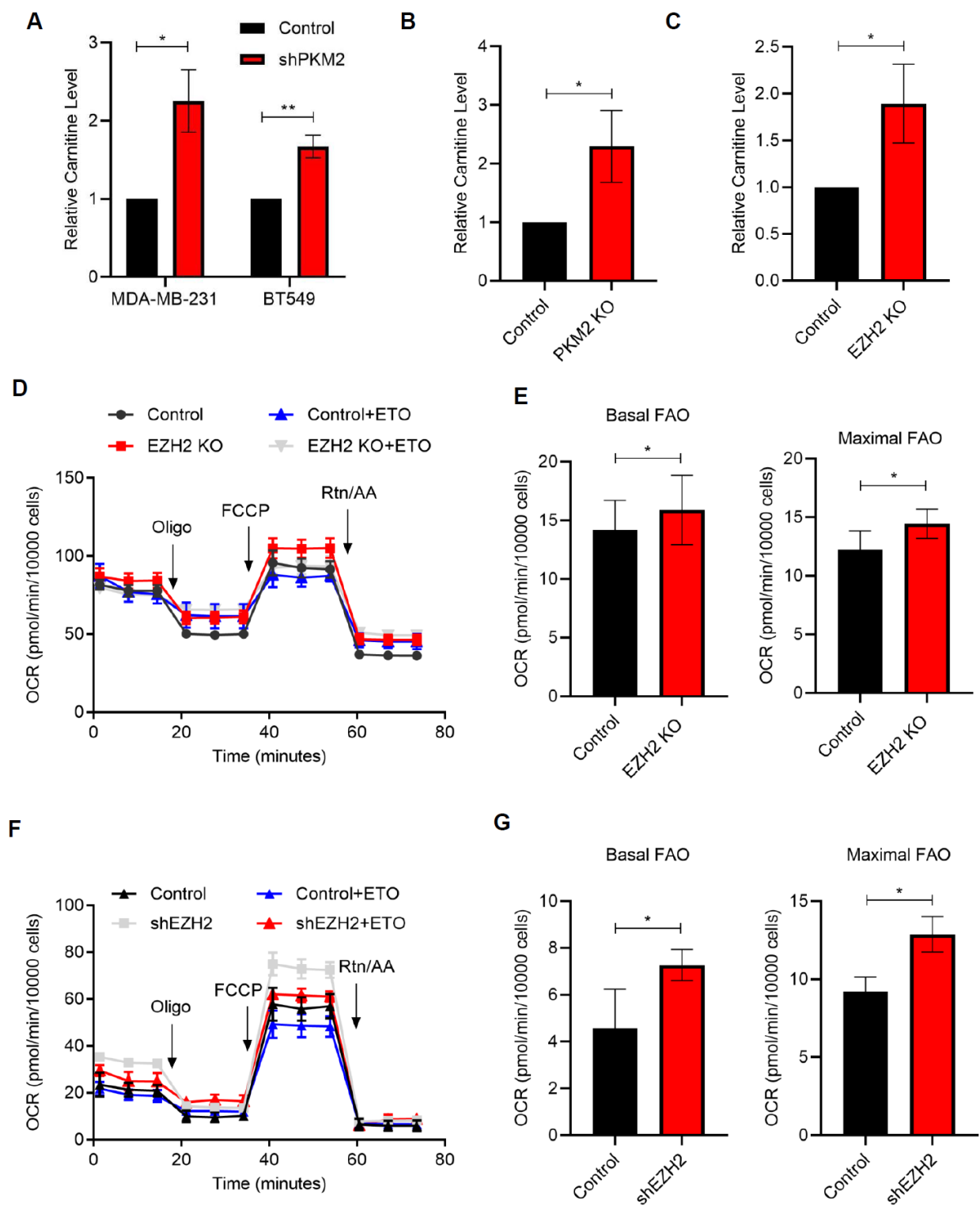
Figure 2-5: Inhibition of PKM2/EZH2 leads to increased intracellular carnitine and enhanced FAO in TNBC cells

Figure 2-5 continued
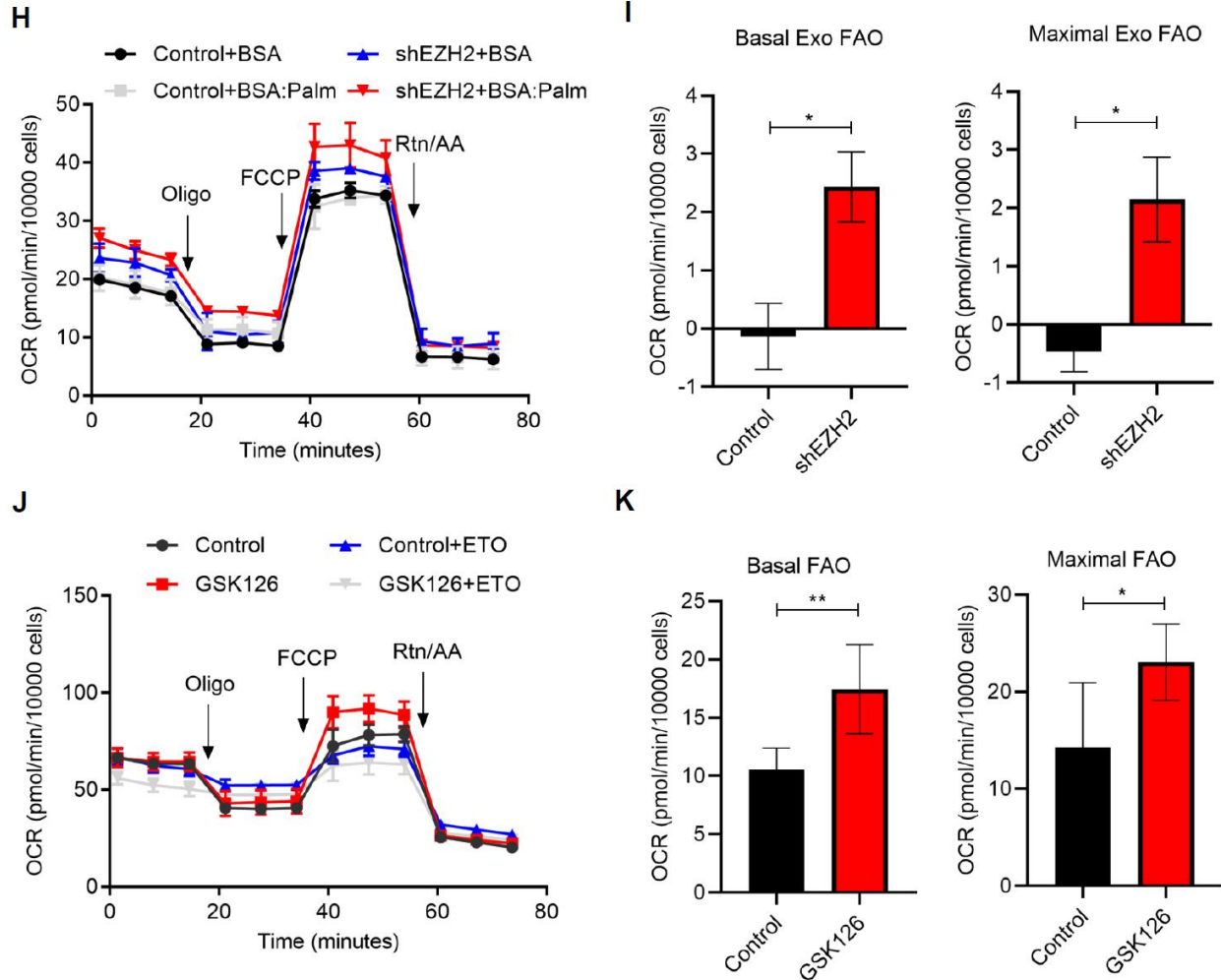
(A-C) Intracellular carnitine level in MDA-MB-231 and BT549 shPKM2 cells (A), MDA-MB-231 PKM2 KO (B) and EZH2 KO (C). (D-G) Endogenous FAO measurement in MDA-MB-231 cells with EZH2 KO (D-E) and EZH2 KD (F-G). (H-I) Exogenous FAO measurement in MDA-MD-231 cells with EZH2 KO. (J-K) Endogenous FAO measurement in MDA-MB-231 treated with 5 μM GSK126 for 3d. Asterisk indicates P<0.05; double asterisks indicate P<0.01. Error bars denote ±SD.

Next, I asked whether enhanced FAO by inhibition of EZH2 could elicit FAO dependency and vulnerability to FAO inhibitor treatment in TNBC cells. Indeed, inhibition of EZH2 expression synergized with Etomoxir in suppressing cell viability and colony formation of MDA-MB-231

cells, where it was shown that a low dose of Etomoxir (<=25 µM), that only exerted a very weak effect in the control cells, was able to significantly hinder cell survival and abolish colony formation upon knockdown of EZH2 (Figure 2-6 A-C). Furthermore, I tested whether there is a synergistic effect of EZH2 and FAO inhibitors on the inhibition of TNBC cell growth. Indeed, single drug treatment exerted only modest inhibition of cell growth of MDA-MB-231, however, combination treatment of either of these two EZH2 inhibitors, GSK126 and Tazemetostat with Etomoxir tremendously impeded cell growth based on two cell viability assays, including CCK8 (a metabolic dependent assay) and SRB (a assay measuring total protein amount). The isobologram graphs of two drugs showed a great synergistic effect of various different concentrations of EZH2 inhibitor combined with Etomoxir. It is worth noting that the synergistic effect was significantly higher with the combinations when the inhibition rate was greater than 80%, which is relevant to clinical therapy (Figure 2-6 D-H). This synergistic effect was further confirmed in another TNBC cells, BT549 (Figure 2-6 I-J). The colony formation assay in MDA-MB-231 and BT549 also demonstrated similar results to MTT results (Figure 2-6 K-L). Just as shPKM2, GSK126 treatment cells rely more on FAO for ATP production (Figure 2-6 M). Together, these data suggest that targeting EZH2 in TNBC cells elicits vulnerability to FAO inhibition.
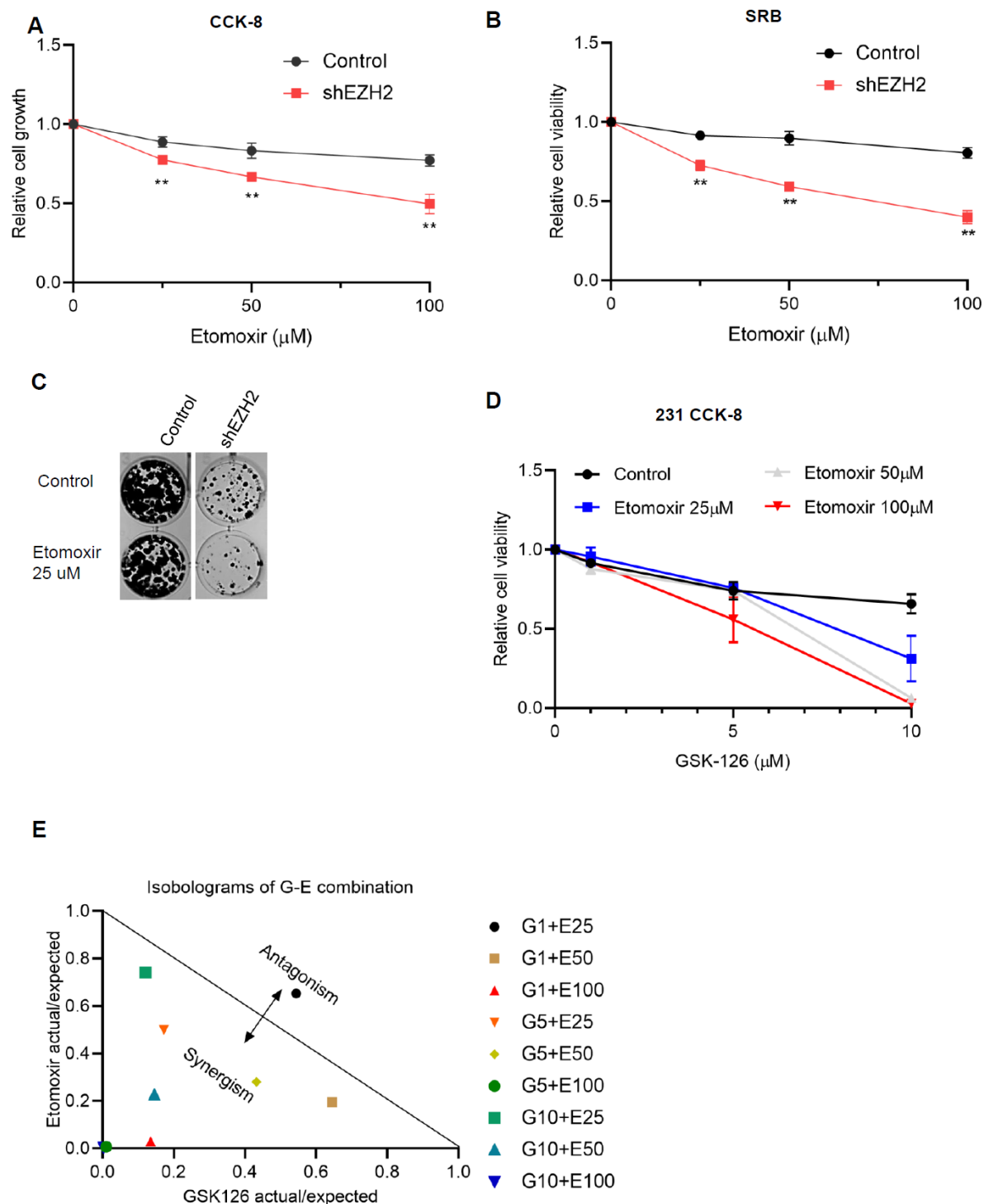
Figure 2-6: Inhibition of EZH2 synergizes with FAO inhibitor in suppressing TNBC cell growth *in vitro*

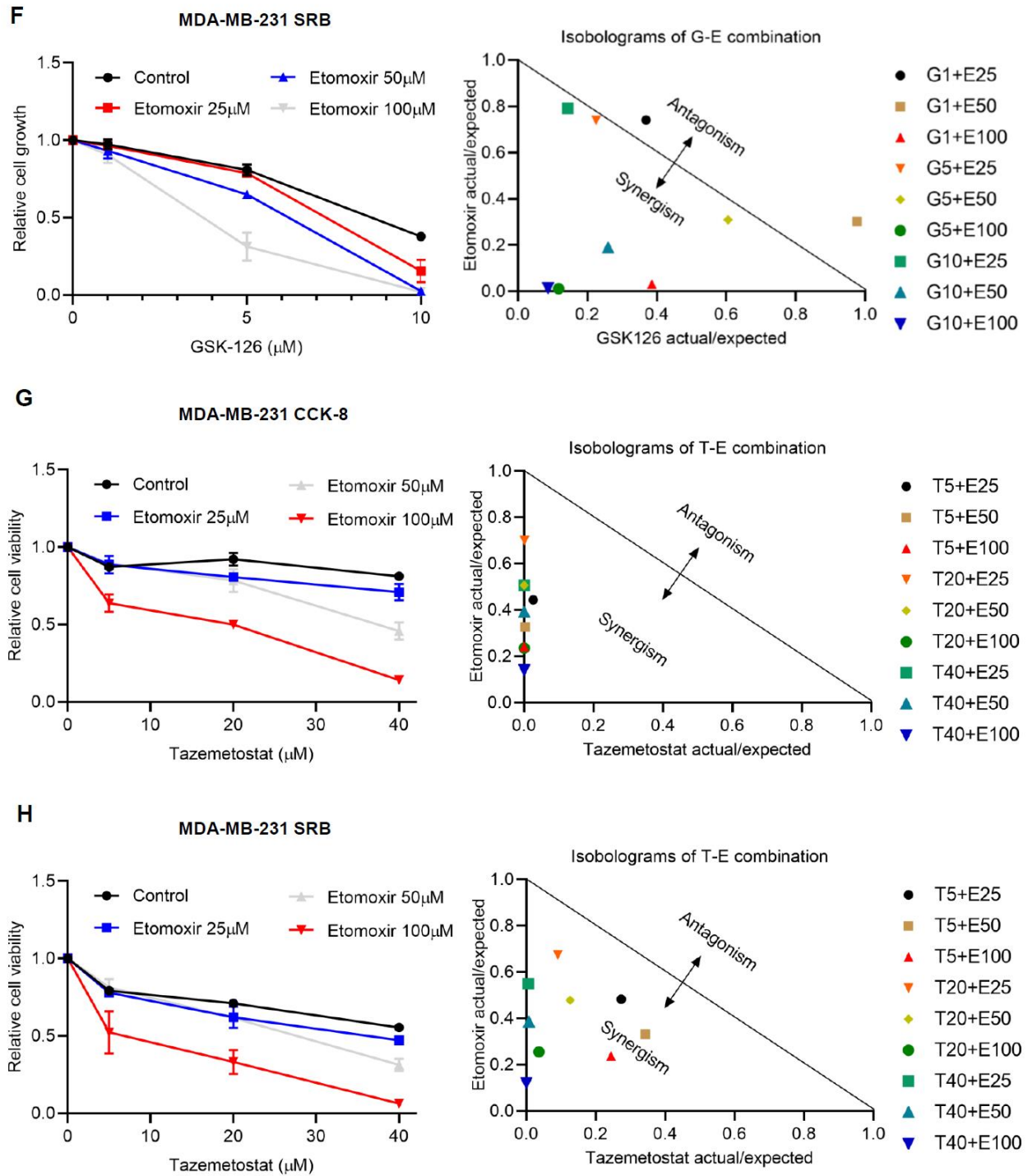Figure 2-6 continued

F

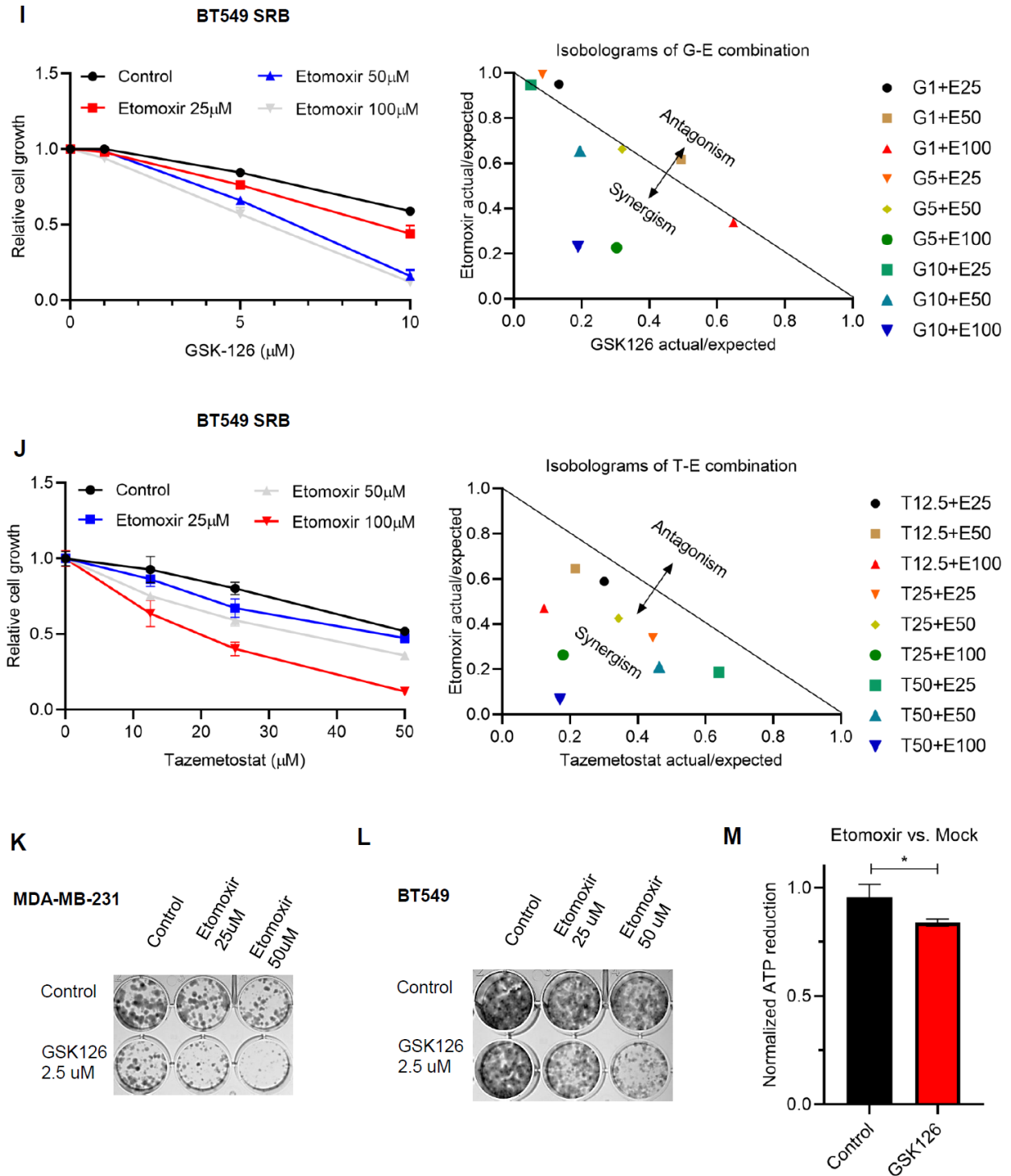
G

H

Figure 2-6 continued

Figure 2-6 continued

(A-B) Cell growth measurement of MDA-MB-231 shEZH2 by either CCK8 or SRB assay after treated with Etomoxir at indicated concentration. (C) Colony formation assay of MDA-MB-231 shEZH2 treated with 25μM Etomoxir. (D) Cell growth measurement of MDA-MB-231 by CCK8 assay after treated with GSK126 with or without Etomoxir at indicated concentration. (E) Isobolograms of the combination effect of GSK126 and Etomoxir in (D). (F) Left: Cell growth measurement of MDA-MB-231 by SRB assay after treated with GSK126 with or without Etomoxir at indicated concentration. Right: Isobolograms of the combination effect of GSK126 and Etomoxir at left. (G-H) Left: Cell growth measurement of MDA-MB-231 by CCK8 assay (G) and SRB assay (H) after treated with Tazemetostat with or without Etomoxir at indicated concentration. Right: Isobolograms of the combination effect of Tazemetostat and Etomoxir at left. (I-J) Left: Cell growth measurement of BT549 by SRB assay after treated with GSK126 (I) or Tazemetostat (J) with or without Etomoxir at indicated concentration. Right: Isobolograms of the combination effect at left. Cell growth curve was normalized to the group without Etomoxir treatment. (K-L) Colony formation assay of MDA-MB-231 (K) and BT549 (L) after treated with GSK126 with or without Etomoxir at indicated concentration. (M) ATP measurement after Etomoxir (50 μM/L) treatment for 1d in MDA-MB-231 cells with or without GSK126 treatment (2.5μM/L) for 2d. Asterisk indicates P<0.05; double asterisks indicate P<0.01. Error bars denote ±SD.

To further determine whether EZH2 inhibitor could sensitize TNBC cells to FAO inhibitor and block tumor progression in vivo, MDA-MB-231 cells that stably expressed luciferase were injected into mammary fat pads of female SCID mice, and when the tumors became palpable, the animals were given GSK126, Etomoxir, GSK126 combined with Etomoxir, or vehicle daily for two weeks. We found that treatment of GSK126 or Etomoxir alone did not have significant effect on xenograft tumor growth, but combined treatment of GSK126 and Etomoxir resulted in significant therapeutic synergism in abrogating tumor growth (Figure 2-7 A-B). Moreover, the expression levels of PKM2 and EZH2 were analyzed in breast cancer patients. High nuclear expression of PKM2 and EZH2 was positively corelated with human breast tumors with high tumor grade (Figure 2-7 C). Together, these data suggest that EZH2 inhibitor elicits a metabolic vulnerability to FAO inhibitor for effective treatment of TNBC (Figure 2-7 D).
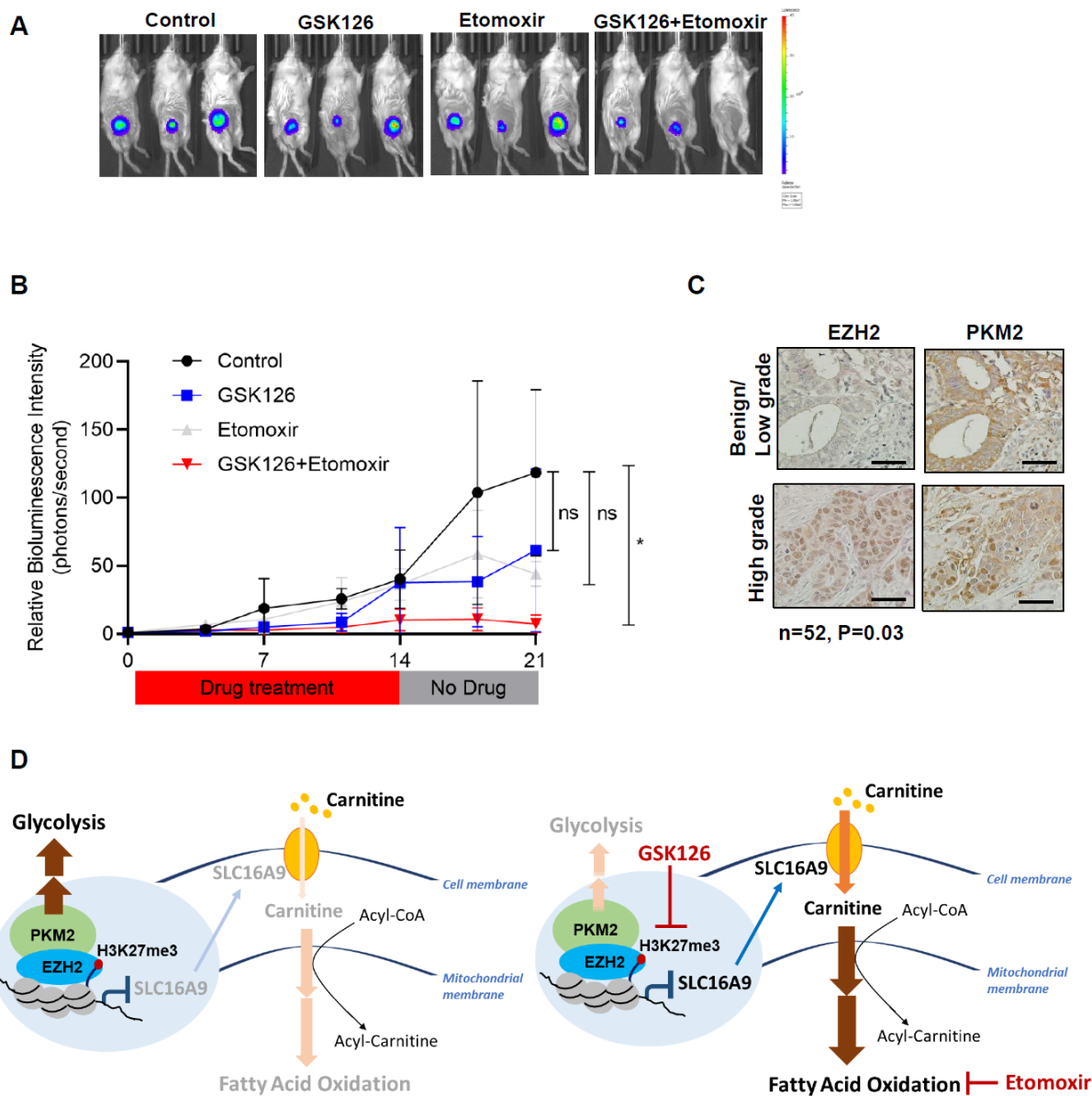
Figure 2-7: EZH2 inhibitor synergizes with FAO inhibitor in suppressing TNBC xenograft tumor growth *in vivo*

(A) The bioluminescent signal at Day 21st in the control group, GSK126 treated group, Etomoxir treated group and GSK126 plus Etomoxir co-treated group. (B) The relative fold change of bioluminescent signal in control and drug treated groups. (C) Representative picture of tissue array staining of breast cancer patient samples. (D) The model of the role of PKM2-EZH2 in metabolic reprogramming in TNBC cells. Asterisk indicates P<0.05. Error bars denote ±SD.

2.4 Discussion

Back in 1960s, Randle discovered the glucose-fatty acid cycle, describing the competition of glucose and fatty acids for the substrate to be oxidized in mitochondrion. Higher level of FAO increases the ratio of NADH/NAD+ and acetyl-CoA/CoA, which allosterically inhibits pyruvate dehydrogenase complex and therefore decrease glucose oxidation. On the contrary, higher level of glucose oxidation leads to the accumulation of malonyl-CoA, which is an allosteric inhibitor of FAO(*85*). However, the regulation at the transcriptional level governing the balance between glucose oxidation and FAO is still unclear. Here I show that inhibition of PKM2 induces the upregulation of genes involved in fatty acid metabolism. The PCR array data demonstrates that PKM2 knock-down increases the expression of genes directly involved in mitochondrial FAO, such as ACADL, ACADS and CPT1C, and peroxisome FAO, such as ACOX2, genes indirectly involved in FAO, such as PRKAA2, which is the catalytic subunit of AMPK that can reduce cellular malonyl-CoA by phosphorylating ACC, and also the genes involved in fatty acid uptake, such as FABP5, FABP6, and LPL (Figure 2-1 E). Furthermore, by carrying out whole-genome ChIP-Seq followed by a qPCR screening, I found that inhibition of PKM2 leads to the enhanced transcription of SLC16A9, a carnitine transporter, resulting in accumulation of carnitine in TNBC cells (Figure 2-4 B and 2-5 A). It is well accepted that PKM2 ablation results in higher OCR. However, this phenomenon contradicts the role of PKM2 as a pyruvate kinase as less PKM2 likely leads to less pyruvate for entering mitochondria to be oxidized. This study likely provides explanation by showing that PKM2 deletion causes accumulation of fatty acid and carnitine (Figure 2-1 F and 2-5 A), along with higher FAO, leading to increased OCR (Figure 2-1 A).

Currently chemotherapy remains the first line treatment for TNBC; however, chemotherapy treated TNBC patients still suffer a higher relapse rate with a worse overall survival compared

48

with other types of breast cancers (1–3). Therefore, there is an urgency for development of new and effective treatments for TNBC. It has been revealed that TNBC cells have a higher glycolysis rate than other types of breast cancer cells. The expression of PKM2, the rate-limiting step enzyme of glycolysis, is inversely correlated with the prognosis of TNBC patients. However, in a TNBC mouse model, the deletion of PKM2 doesn't hinder or slow down the tumorigenesis, suggesting that TNBC cells can develop an alternative pathway to bypass the requirement of glycolysis for cancer progression; the underlying mechanism is not yet clear.

In this study, I have found that inhibition of PKM2, activates a metabolic switch from glycolysis dependency to FAO dependency in triple-negative breast cancer cells. Mechanistically, I have shown that PKM2 directly interacts with EZH2 to coordinately mediate epigenetic silencing of the transcription of SLC16A9, which is a transporter of Carnitine, the key substrate of fatty acid oxidation (FAO). Ablation of PKM2 or EZH2 increases expression of SLC16A9 and intracellular Carnitine level, and therefore enhances endogenous FAO. Furthermore, ablation of either PKM2 or EZH2, TNBC cells become more dependent on FAO and develop vulnerability to FAO inhibition. Although both GSK126, a EZH2 inhibitor, and Etomoxir, a FAO inhibitor, have been tested in clinical trials as single agents, it is worth noting that GSK126 alone has only shown therapeutic effects in hematopoietic malignancies but not in solid tumors, and high concentration of Etomoxir is known to cause liver toxicity and result in off-target effects (*62, 86–88*). In this study, I have shown that compared with single agent treatment, the newly developed GSK126-Etomoxir combination strategy significantly enhances therapeutic potency with low doses in the pre-clinical model. Overall, this study not only for the first time reveals an epigenetic regulation

of the balance between glycolysis and FAO, but also suggests a new drug combination therapy that can be readily applied to TNBC patients.

CHAPTER 3.   THE ROLE OF EZH2 IN THE METABOLIC REGULATION OF THE MATURATION OF DENDRITIC CELLS

3.1   Introduction

Dendritic cells (DC) are the most professional type of antigen presenting cells (*89*). There are three types of DCs in mammals, conventional DCs (cDCs), plasmacytoid DCs (pDCs), and monocyte-derived DCs (moDCs). cDCs and pDCs are derived in bone marrow under the control of lineage specific transcription factor, Id-2 and E2-2 respectively. moDCs originate from monocytes and differentiate into DC in tissues. When tumor cells die, DC takes up tumor cell debris, digests and presents tumor cell neo-antigens to cytotoxic T cells and initiate antigen specific anti-tumor immune response. Under the steady state, moDCs are absent but become significantly increased following inflammation, infection, or tumorigenesis, playing an important role in the activation of cancer immunity (*90, 91*). It has also been shown that DC vaccination derived from moDCs provides promising results in treating cancer patients (*90, 92*). However, *in vitro* generation of fully functional DC remains a big challenge in this field because current protocols for deriving DC compromise either the production of interleukin-12p70 (IL-12p70) for gold standard DC (sDC) or the sensitivity to recruitment signal to secondary lymphoid organs for α-type 1-polarized-DC (αDC)(*93*). EZH2 inhibition has shown to be able to create an immunologically hot tumor microenvironment(*66, 94*). However, the underlying mechanism for the reprogramming process is still unclear. This study aims to investigate whether EZH2 participates the DC maturation process and benefits *in vitro* derivation of fully functional DC. I have found that the expression levels of EZH2 and its functional maker, H3K27Me3, are upregulated following the maturation from immature DC (iDC) into two functional DCs, αDC and sDC. Moreover, EZH2 inhibition by

GSK126 elicits a higher dependency on FAO in sDC than αDC/iDC. These results suggest that EZH2 may affect DC maturation through reprogramming DC metabolism.

3.2 Material and Methods

3.2.1 Generation of Dendritic Cells

Dendritic Cells were kindly provided by Mr. Bowen Dong from Dr. Pawel Kalinski's lab at Roswell Park Cancer Institute according to the previously reported method (*93*). Briefly, peripheral blood mononuclear cells (PBMCs) donated by healthy donors were isolated with lymphocyte separation medium (Cellgro Mediatech). Monocytes were isolated by density gradients centrifugation with Percoll (Sigma) followed by plastic adherence. iDCs were derived from monocytes after being cultured with GM-CSF and IL-4 (both 1,000 IU/mL) for six days. iDCs were then treated with or without GSK126 (5μM/L) for three days followed by incubation with different maturation cocktails for 18 hours for the maturation of either sDCs or αDCs. For the maturation of sDCs, the maturation cocktail consists of IL-1β (25 ng/mL), TNFα (50 ng/mL), IL-6 (1,000 units/mL), and PGE2 (106 mol/L). For the maturation of αDCs, the maturation regimen consists of IL-1β (25 ng/mL), TNFα (50 ng/mL), poly-I:C (20g/mL), IFNα (3,000 units/mL), and IFNγ (1,000 units/mL).

3.2.2 Seahorse Extracellular Flux analysis

60000 iDCs, sDCs, and αDCs were seeded per well in XF96 assay plates (Agilent, 101085-004) coated with Cell-Tak (Corning, Cat. # 354240) to immobilize suspension cells in DMEM (pH 7.4) supplemented with 25mM Glucose, 2mM Glutamine, and 1mM Pyruvate. For endogenous FAO measurement, 15 min before assay, Etomoxir was manually added into related wells at a final concentration of 50μM. During the assay, oxygen consumption (OCR) was measured at basal

status and after Mito Stress Test compounds treatment (2μM oligomycin, 1μM FCCP and 1μM rotenone and antimycin A was injected into designed wells by the machine at indicated time points). Basal respiration was calculated by the OCR at basal status minus the OCR after the addition of rotenone and antimycin A. Maximal respiration was calculated by the OCR after FCCP treatment subtracts the OCR after the addition of rotenone and antimycin A. For glycolysis measurement, proton efflux rate (PER) was measured under both basal condition and in response to 0.5μM rotenone and antimycin A, and 50mM 2-DG.

3.2.3   Immunoblot

iDCs, sDCs, and αDCs were lysed in 1X lysis buffer (CST, 9803) with supplements of protease inhibitor cocktail (GenDEPOT, P3100) and phosphatase inhibitor cocktail (BOXTER, AR1183). Lysate were then sonicated and pelleted. Supernatant was collected and protein was quantified by Pierce™ BCA Protein Assay Kit (Thermo Fisher Scientific, 23225). Samples were boiled in 1X Loading buffer for 5 min. After placing on ice for 5 min, samples were loaded into SDS-PAGE and immunoblotted by interested antibodies with dilution as following: EZH2 mAb (CST, 5246) at 1:2000, Histone H3 mAb (CST, 4499) at 1:3000, Tri-Methyl-Histone H3 (Lys27) mAb (CST, 9733) at 1:1000, Actin mAb (Sigma, A5441) at 1:5000.

3.3   Results

To understand whether EZH2 has a role in maturation of DC, I first compared the protein levels of EZH2 and its functional marker H3K27Me3 in iDC, αDC and sDC. As shown in Figure 3-1 A, the expression of EZH2 and H3K27Me3 levels were enhanced in both αDC and sDC compared to iDC, suggesting that EZH2 mediated epigenetic regulation may play a role in the maturation of iDC into functional DCs. It has been shown that the function of DC is tightly correlated with their

metabolic phenotype. Next, I investigated differential metabolic profiles between these three DCs and whether EZH2 indeed played a role in the metabolic regulation. I found that compared with αDC and iDC, sDC had stronger glycolysis and mitochondrial respiration, which were sensitive to the inhibition of EZH2 with GSK126 treatment. Moreover, GSK126 did not elicit significant effects on glycolysis and mitochondrial respiration in αDC and iDC (Figure 3-1 B and C). Together, these data suggest that EZH2 may play a role in metabolic regulation of DC, especially in sDC.
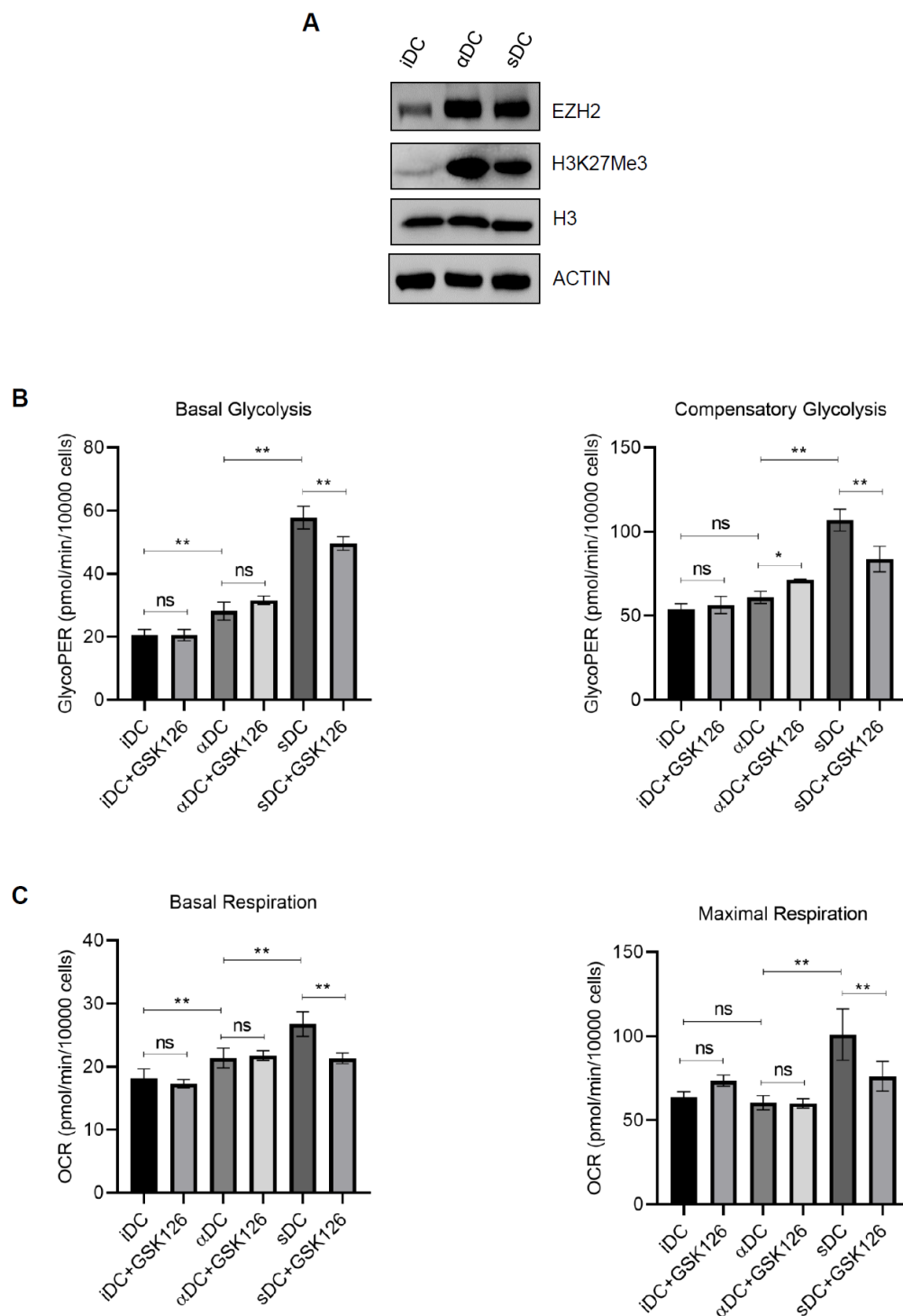
Figure 3-1: Correlation of EZH2 expression/activity with metabolic states in three different DCs

(A) EZH2 expression and H3K27Me3 level in three different DCs (B) Glycolysis (C) and mitochondrial respiration (OCR) analysis in three different DCs with or without 5μM GSK126 treatment for 3d.

As it was shown in the Chapter 2 that EZH2 has an effect on fatty acid oxidation (FAO) in TNBC, we inquired how EZH2 was involved in FAO of DCs. We found that GSK126 treatment didn't affect FAO in iDC (Figure 3-2 A). However, in both αDC and sDC, EZH2 inhibition caused a reduction in FAO but the functional effects may be different. In αDC, GSK126 treatment didn't change its basal respiration suggesting that the FAO reduction caused by EZH2 inhibition could be compensated by utilization of other fuels, such as pyruvate or glutamate. However, in sDC, the reduction of FAO resulted in a declined basal respiration, indicating that this reduction could not be compensated, and therefore EZH2 inhibition could lead to a significantly functional change in sDC (Figure 3-2 B and C). We next tested whether EZH2 affected maturation of DCs by examining MFI ratio of the expression of CD80, CD86, CD83 and MHC-II on sDC and αDC with or without 5 µM/L GSK126 treatment for three days. We found that the inhibition of EZH2 did not change the expression levels of co-stimulatory factors, CD80, CD83 and CD86, or MHC-II in sDC and αDC, suggesting that EZH2 may not affect the maturation process of DCs (data not shown). We will be interrogating whether EZH2 mediated metabolic regulation could contribute to the functional differences in sDC and αDC, such as migratory potential and cytokine production, that would impact antigen specific T cell activation.
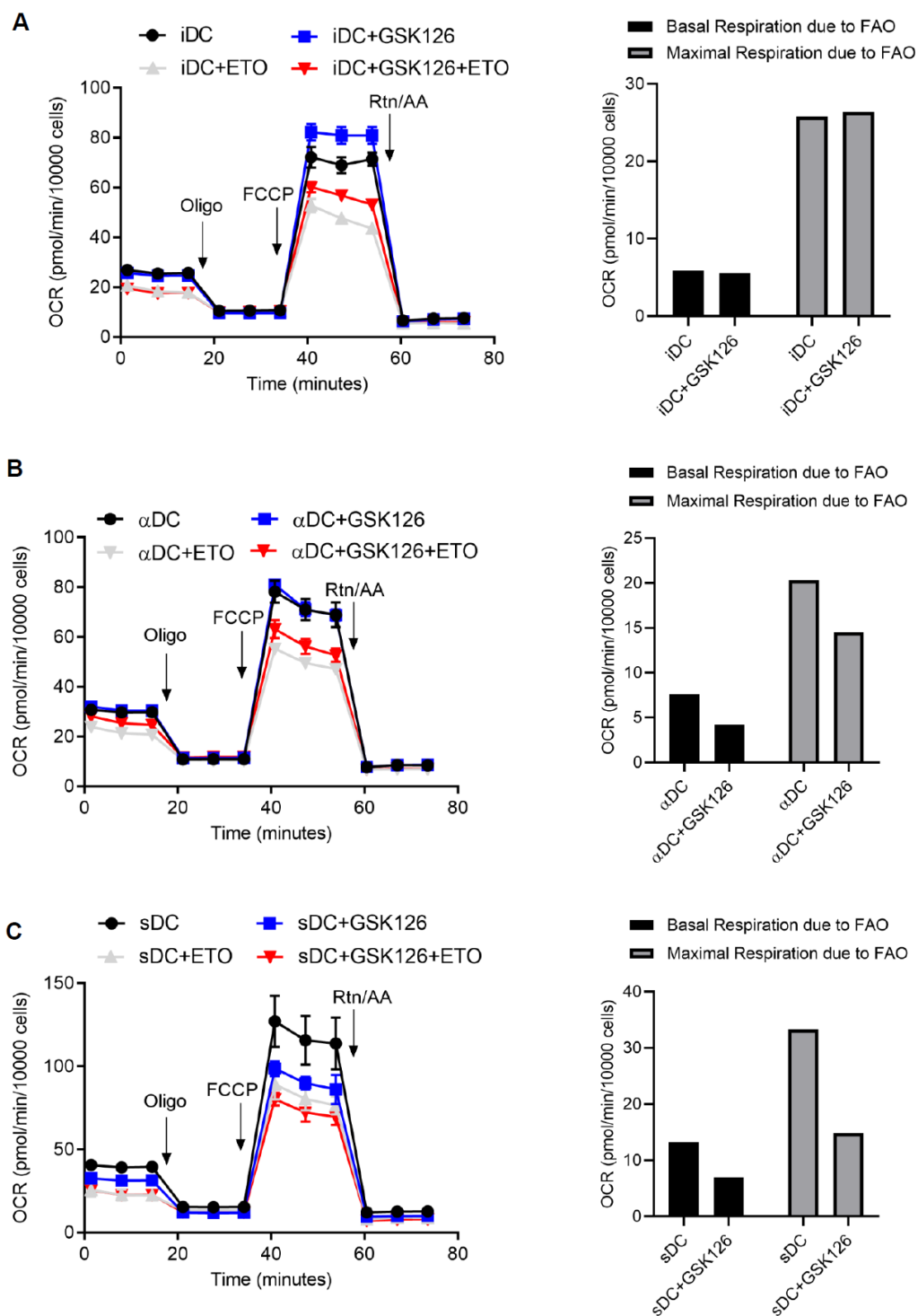
Figure 3-2: The effect of EZH2 inhibition on FAO in three different DCs

(A-C) Measurement of FAO in (A) iDC, (B) αDC, and (C) sDC with or without 5μM GSK126 treatment for three days.

3.4 Discussion

EZH2 has been shown to be important for maintaining the function and the population Treg cells through maintain the expression of Foxp3 and therefore to sustain the homeostasis of immune system(*64*, *65*). Moreover, a recent study combining immune checkpoint blockade with the EZH2 inhibitor, CPI-1205, showed that there is a strong synergism between these two treatments, suggesting the inhibition of EZH2 reprograms the immunologically cold microenvironment to a hot microenvironment(*66*). However, the role of EZH2 in regulation of dendritic cells is not clear. Here, I demonstrate that during the maturation process of DC, EZH2 expression is upregulated and H3K27Me3 level is also increased, suggesting EZH2 mediated epigenetic regulation may participate in the process. Moreover, as it has been shown that the function of DC is tightly correlated with their metabolic phenotype, I tested glycolysis and mitochondrial respiration of three types of DCs in vitro, and found that iDC, αDC and sDC have totally different metabolic phenotypes. iDC has the lowest metabolic rate (both glycolysis and mitochondrial respiration), αDC has the medium metabolic rate, and sDC has the highest metabolic rate. Moreover, EZH2 inhibition causes a reduction of metabolic rate in sDC, but not in the other two DCs. Furthermore, the decrease of basal respiration upon EZH2 inhibition in sDC is mainly due to a reduction of FAO. Overall, these data imply that the role of EZH2 in different types of DCs may be functionally linked. Although EZH2 does not have a significant effect on maturation of sDC and αDC as shown by the expression levels of co-stimulatory factors, CD80, CD83 and CD86, and MHC-II, EZH2 may still play a role in DC's capability to activate antigen specific T cells, such as by affecting the production of IL-12 and recruitment response to secondary lymphoid organs. Therefore, future studies will be pursued to address how EZH2 affects migratory potential and cytokine production of both sDC and αDC, and therefore impacts antigen specific T cell activation.

REFERENCES

1. G. Bianchini, J. M. Balko, I. A. Mayer, M. E. Sanders, L. Gianni, Triple-negative breast cancer: challenges and opportunities of a heterogeneous disease. *Nat. Rev. Clin. Oncol.* **13**, 674–690 (2016).

2. W. D. Foulkes, I. E. Smith, J. S. Reis-Filho, Triple-Negative Breast Cancer. *N. Engl. J. Med.* **363**, 1938–1948 (2010).

3. R. Dent *et al.*, Triple-negative breast cancer: clinical features and patterns of recurrence. *Clin. Cancer Res.* **13**, 4429–34 (2007).

4. A. G. Waks, E. P. Winer, Breast Cancer Treatment: A Review. *JAMA - J. Am. Med. Assoc.* **321** (2019), pp. 288–300.

5. H. Joshi, M. F. Press, in *The Breast: Comprehensive Management of Benign and Malignant Diseases* (Elsevier Inc., 2018), pp. 282-307.e5.

6. N. E. Ben-Baruch, R. Bose, S. M. Kavuri, C. X. Ma, M. J. Ellis, HER2-mutated breast cancer responds to treatment with single-agent neratinib, a second-generation HER2/EGFR tyrosine kinase inhibitor. *JNCCN J. Natl. Compr. Cancer Netw.* **13**, 1061–1064 (2015).

7. K. Albain *et al.*, Comparisons between different polychemotherapy regimens for early breast cancer: Meta-analyses of long-term outcome among 100 000 women in 123 randomised trials. *Lancet.* **379**, 432–444 (2012).

8. J. L. Blum *et al.*, in *Journal of Clinical Oncology* (American Society of Clinical Oncology, 2017), vol. 35, pp. 2647–2655.

9. M. Chavez-MacGregor *et al.*, Incorporating Tumor Characteristics to the American Joint Committee on Cancer Breast Cancer Staging System. *Oncologist.* **22**, 1292–1300 (2017).

10. W. G. Kaelin, The concept of synthetic lethality in the context of anticancer therapy. *Nat. Rev. Cancer.* **5** (2005), pp. 689–698.

11. J. K. Litton *et al.*, Talazoparib in Patients with Advanced Breast Cancer and a Germline BRCA Mutation. *N. Engl. J. Med.* **379**, 753–763 (2018).

12. M. Robson *et al.*, Olaparib for Metastatic Breast Cancer in Patients with a Germline BRCA Mutation. *N. Engl. J. Med.* **377**, 523–533 (2017).

13. D. Hanahan, R. A. Weinberg, Hallmarks of Cancer: The Next Generation. *Cell.* **144**, 646–674 (2011).

14. B. Altenberg, K. O. Greulich, Genes of glycolysis are ubiquitously overexpressed in 24 cancer classes. *Genomics*. **84**, 1014–1020 (2004).

15. M. Tamada, M. Suematsu, H. Saya, Pyruvate kinase M2: multiple faces for conferring benefits on cancer cells. *Clin. Cancer Res.* **18**, 5554–61 (2012).

16. H. R. Christofk *et al.*, The M2 splice isoform of pyruvate kinase is important for cancer metabolism and tumour growth. *Nature*. **452**, 230–233 (2008).

17. S. Mazurek, C. B. Boschek, F. Hugo, E. Eigenbrodt, Pyruvate kinase type M2 and its role in tumor growth and spreading. *Semin. Cancer Biol.* **15**, 300–308 (2005).

18. T. Hitosugi *et al.*, Tyrosine phosphorylation inhibits PKM2 to promote the warburg effect and tumor growth. *Sci. Signal.* **2** (2009), doi:10.1126/scisignal.2000431.

19. Z. Zhou *et al.*, Oncogenic Kinase–Induced PKM2 Tyrosine 105 Phosphorylation Converts Nononcogenic PKM2 to a Tumor Promoter and Induces Cancer Stem–like Cells. *Cancer Res.* **78**, 2248–2261 (2018).

20. H. R. Christofk, M. G. Vander Heiden, N. Wu, J. M. Asara, L. C. Cantley, Pyruvate kinase M2 is a phosphotyrosine-binding protein. *Nature*. **452**, 181–186 (2008).

21. L. Lv *et al.*, Mitogenic and Oncogenic Stimulation of K433 Acetylation Promotes PKM2 Protein Kinase Activity and Nuclear Localization. *Mol. Cell*. **52**, 340–352 (2013).

22. W. Yang *et al.*, PKM2 phosphorylates histone H3 and promotes gene transcription and tumorigenesis. *Cell*. **150**, 685–696 (2012).

23. K. Suhre *et al.*, Human metabolic individuality in biomedical and pharmaceutical research. *Nature*. **477**, 54–60 (2011).

24. X. Gao, H. Wang, J. J. Yang, X. Liu, Z.-R. Liu, Pyruvate Kinase M2 Regulates Gene Transcription by Acting as a Protein Kinase. *Mol. Cell*. **45**, 598–609 (2012).

25. W. Yang *et al.*, Nuclear PKM2 regulates β-catenin transactivation upon EGFR activation. *Nature*. **480**, 118–122 (2011).

26. F. Liu *et al.*, PKM2 methylation by CARM1 activates aerobic glycolysis to promote tumorigenesis. *Nat. Cell Biol.* **19**, 1358–1370 (2017).

27. W. J. Israelsen *et al.*, PKM2 Isoform-Specific Deletion Reveals a Differential Requirement for Pyruvate Kinase in Tumor Cells. *Cell*. **155**, 397–409 (2013).

28. T. L. Dayton *et al.*, Isoform-specific deletion of PKM2 constrains tumor initiation in a mouse model of soft tissue sarcoma. *Cancer Metab.* **6**, 6 (2018).

29. T. L. Dayton *et al.*, Germline loss of PKM2 promotes metabolic distress and hepatocellular carcinoma. *Genes Dev.* **30**, 1020–33 (2016).

30. M. Cortés-Cros *et al.*, M2 isoform of pyruvate kinase is dispensable for tumor maintenance and growth. *Proc. Natl. Acad. Sci.* **110**, 489–494 (2013).

31. D. Anastasiou *et al.*, Pyruvate kinase M2 activators promote tetramer formation and suppress tumorigenesis. *Nat. Chem. Biol.* **8**, 839–847 (2012).

32. D. Pouessel *et al.*, "PHASE II STUDY OF TLN-232*, A NOVEL M2PK TARGETING AGENT, ADMINISTERED BY CIV TO PATIENTS WITH ADVANCED RENAL CELL CARCINOMA (RCC)," (available at www.thallion.com).

33. Epigenetics: A Landscape Takes Shape. *Cell*. **128**, 635–638 (2007).

34. Histone modifications in transcriptional regulation. *Curr. Opin. Genet. Dev.* **12**, 142–148 (2002).

35. Functional consequences of histone modifications. *Curr. Opin. Genet. Dev.* **13**, 154–160 (2003).

36. H. Yamaguchi, M.-C. Hung, Regulation and Role of EZH2 in Cancer. *Cancer Res. Treat.* **46**, 209–22 (2014).

37. The functions of E(Z)/EZH2-mediated methylation of lysine 27 in histone H3. *Curr. Opin. Genet. Dev.* **14**, 155–164 (2004).

38. S. Aranda, G. Mas, L. Di Croce, Regulation of gene transcription by Polycomb proteins. *Sci. Adv.* **1**, e1500737 (2015).

39. R. A. Gupta *et al.*, Long non-coding RNA HOTAIR reprograms chromatin state to promote cancer metastasis. *Nature*. **464**, 1071–1076 (2010).

40. J. Zhao, B. K. Sun, J. A. Erwin, J. J. Song, J. T. Lee, Polycomb proteins targeted by a short repeat RNA to the mouse X chromosome. *Science (80-.).* **322**, 750–756 (2008).

41. S. Kaneko *et al.*, Phosphorylation of the PRC2 component Ezh2 is cell cycle-regulated and up-regulates its binding to ncRNA. *Genes Dev.* **24**, 2615–2620 (2010).

42. R. Margueron, D. Reinberg, The Polycomb complex PRC2 and its mark in life. *Nature*. **469** (2011), pp. 343–349.

43. T. Ernst *et al.*, Inactivating mutations of the histone methyltransferase gene EZH2 in myeloid disorders. *Nat. Genet.* **42**, 722–726 (2010).

44. L. Herviou, G. Cavalli, G. Cartron, B. Klein, J. Moreaux, EZH2 in normal hematopoiesis and hematological malignancies. *Oncotarget*. **7**, 2284–2296 (2016).

45. S. Varambally *et al.*, The polycomb group protein EZH2 is involved in progression of prostate cancer. *Nature*. **419**, 624–629 (2002).

46. I. M. Bachmann *et al.*, EZH2 expression is associated with high proliferation rate and aggressive tumor subgroups in cutaneous melanoma and cancers of the endometrium, prostate, and breast. *J. Clin. Oncol.* **24**, 268–73 (2006).

47. R. D. Morin *et al.*, Somatic mutations altering EZH2 (Tyr641) in follicular and diffuse large B-cell lymphomas of germinal-center origin. *Nat. Genet.* **42**, 181–185 (2010).

48. C. J. Sneeringer *et al.*, Coordinated activities of wild-type plus mutant EZH2 drive tumor-associated hypertrimethylation of lysine 27 on histone H3 (H3K27) in human B-cell lymphomas. *Proc. Natl. Acad. Sci. U. S. A.* **107**, 20980–5 (2010).

49. D. B. Yap *et al.*, Somatic mutations at EZH2 Y641 act dominantly through a mechanism of selectively altered PRC2 catalytic activity, to increase H3K27 trimethylation. *Blood*. **117**, 2451–2459 (2011).

50. L. P. Kunju *et al.*, EZH2 and ALDH-1 mark breast epithelium at risk for breast cancer development. *Mod. Pathol.* **24**, 786–793 (2011).

51. L. Ding, C. Erdmann, A. M. Chinnaiyan, S. D. Merajver, C. G. Kleer, Identification of EZH2 as a Molecular Marker for a Precancerous State in Morphologically Normal Breast Tissues. *Cancer Res* (2006), doi:10.1158/0008-5472.CAN-05-4300.

52. F. M. Raaphorst *et al.*, Poorly Differentiated Breast Carcinoma is Associated with Increased Expression of the Human Polycomb Group EZH2 Gene. *Neoplasia*. **5**, 481–488 (2003).

53. A. M. Pietersen *et al.*, EZH2 and BMI1 inversely correlate with prognosis and TP53 mutation in breast cancer. *Breast Cancer Res.* **10**, R109 (2008).

54. K. Holm *et al.*, Global H3K27 trimethylation and EZH2 abundance in breast tumor subtypes. *Mol. Oncol.* **6**, 494–506 (2012).

55. C. G. Kleer *et al.*, EZH2 is a marker of aggressive breast cancer and promotes neoplastic transformation of breast epithelial cells. *Proc. Natl. Acad. Sci. U. S. A.* **100**, 11606–11 (2003).

56. S. Fujii, K. Ito, Y. Ito, A. Ochiai, Enhancer of zeste homologue 2 (EZH2) down-regulates RUNX3 by increasing histone H3 methylation. *J. Biol. Chem.* **283**, 17324–32 (2008).

57.   X. Yang *et al.*, CDKN1C (p57KIP2) Is a Direct Target of EZH2 and Suppressed by Multiple Epigenetic Mechanisms in Breast Cancer Cells. *PLoS One*. **4**, e5011 (2009).

58.   J. Du *et al.*, FOXC1, a target of polycomb, inhibits metastasis of breast cancer cells. *Breast Cancer Res. Treat.* **131**, 65–73 (2012).

59.   Q. Cao *et al.*, Repression of E-cadherin by the polycomb group protein EZH2 in cancer. *Oncogene*. **27**, 7274–7284 (2008).

60.   G. Ren *et al.*, Polycomb Protein EZH2 Regulates Tumor Invasion via the Transcriptional Repression of the Metastasis Suppressor RKIP in Breast and Prostate Cancer. *Cancer Res.* **72**, 3091–3104 (2012).

61.   EZH2 Promotes Expansion of Breast Tumor Initiating Cells through Activation of RAF1-β-Catenin Signaling. *Cancer Cell*. **19**, 86–100 (2011).

62.   N. Gulati, W. Béguelin, L. Giulino-Roth, Enhancer of zeste homolog 2 (EZH2) inhibitors. *Leuk. Lymphoma*. **59** (2018), pp. 1574–1585.

63.   M. DuPage *et al.*, The chromatin-modifying enzyme Ezh2 is critical for the maintenance of regulatory T cell identity after activation. *Immunity*. **42**, 227–238 (2015).

64.   X. P. Yang *et al.*, EZH2 is crucial for both differentiation of regulatory T cells and T effector cell expansion. *Sci. Rep.* **5** (2015), doi:10.1038/srep10643.

65.   D. Wang *et al.*, Targeting EZH2 Reprograms Intratumoral Regulatory T Cells to Enhance Cancer Immunity. *Cell Rep.* **23**, 3262–3274 (2018).

66.   S. Goswami *et al.*, Modulation of EZH2 expression in T cells improves efficacy of anti-CTLA-4 therapy. *J. Clin. Invest.* **128**, 3813–3818 (2018).

67.   P. Rinaldo, D. Matern, M. J. Bennett, Fatty Acid Oxidation Disorders. *Annu. Rev. Physiol.* **64**, 477–502 (2002).

68.   U. Harjes, J. Kalucka, P. Carmeliet, Targeting fatty acid metabolism in cancer and endothelial cells. *Crit. Rev. Oncol. Hematol.* **97** (2016), pp. 15–21.

69.   N. F. Brown *et al.*, Mouse white adipocytes and 3T3-L1 cells display an anomalous pattern of carnitine palmitoyltransferase (CPT) I isoform expression during differentiation. Inter-tissue and inter-species expression of CPT I and CPT II enzymes. *Biochem. J.* **327**, 225–231 (1997).

70.   N. T. Price *et al.*, A novel brain-expressed protein related to carnitine palmitoyltransferase I. *Genomics*. **80**, 433–442 (2002).

71.   P. Rinaldo, D. Matern, M. J. Bennett, F ATTY A CID O XIDATION D ISORDERS. *Annu. Rev. Physiol.* **64**, 477–502 (2002).

72.   A. Carracedo, L. C. Cantley, P. P. Pandolfi, Cancer metabolism: Fatty acid oxidation in the limelight. *Nat. Rev. Cancer.* **13**, 227–232 (2013).

73.   K. Zaugg *et al.*, Carnitine palmitoyltransferase 1C promotes cell survival and tumor growth under conditions of metabolic stress. *Genes Dev.* **25**, 1041–1051 (2011).

74.   P. Caro *et al.*, Metabolic Signatures Uncover Distinct Targets in Molecular Subsets of Diffuse Large B Cell Lymphoma. *Cancer Cell.* **22**, 547–560 (2012).

75.   I. Samudio *et al.*, Pharmacologic inhibition of fatty acid oxidation sensitizes human leukemia cells to apoptosis induction. *J. Clin. Invest.* **120**, 142–156 (2010).

76.   Y. nan Wang *et al.*, CPT1A-mediated fatty acid oxidation promotes colorectal cancer cell metastasis by inhibiting anoikis. *Oncogene.* **37**, 6025–6040 (2018).

77.   J. Shen, L. Yan, S. Liu, C. B. Ambrosone, H. Zhao, Plasma metabolomic profiles in breast cancer patients and healthy controls: By race and tumor receptor subtypes. *Transl. Oncol.* **6**, 757–765 (2013).

78.   T. Wang *et al.*, JAK/STAT3-Regulated Fatty Acid β-Oxidation Is Critical for Breast Cancer Stem Cell Self-Renewal and Chemoresistance. *Cell Metab.* **27**, 136-150.e5 (2018).

79.   R. Camarda *et al.*, Inhibition of fatty acid oxidation as a therapy for MYC-overexpressing triple-negative breast cancer. *Nat. Med.* **22**, 427–432 (2016).

80.   W. Luo *et al.*, Pyruvate Kinase M2 Is a PHD3-Stimulated Coactivator for Hypoxia-Inducible Factor 1. *Cell.* **145**, 732–744 (2011).

81.   T. L. Dayton, T. Jacks, M. G. Vander Heiden, PKM2, cancer metabolism, and the road ahead. *EMBO Rep.* **17**, 1721–1730 (2016).

82.   V. Vichai, K. Kirtikara, Sulforhodamine B colorimetric assay for cytotoxicity screening. *Nat. Protoc.* **1**, 1112–1116 (2006).

83.   Inhibition of fatty acid oxidation by etomoxir impairs NADPH production and increases reactive oxygen species resulting in ATP depletion and cell death in human glioblastoma cells - ScienceDirect, (available at https://www.sciencedirect.com/science/article/pii/S0005272810007401).

84. L. Benetatos, E. Voulgaris, G. Vartholomatos, E. Hatzimichael, Non-coding RNAs and EZH2 interactions in cancer: Long and short tales from the transcriptome. *Int. J. Cancer.* **133**, 267–274 (2013).

85. P. J. Randle, Regulatory interactions between lipids and carbohydrates: The glucose fatty acid cycle after 35 years. *Diabetes. Metab. Rev.* **14** (1998), pp. 263–283.

86. B. Raud *et al.*, Etomoxir Actions on Regulatory and Memory T Cells Are Independent of Cpt1a-Mediated Fatty Acid Oxidation. *Cell Metab.* **28**, 504-515.e7 (2018).

87. A. S. Divakaruni *et al.*, Etomoxir Inhibits Macrophage Polarization by Disrupting CoA Homeostasis. *Cell Metab.* **28**, 490-503.e7 (2018).

88. C. J. F. Holubarsch *et al.*, A double-blind randomized multicentre clinical trial to evaluate the efficacy and safety of two doses of etomoxir in comparison with placebo in patients with moderate congestive heart failure: the ERGO (etomoxir for the recovery of glucose oxidation) stud. *Clin. Sci.* **113**, 205–212 (2007).

89. A. Alloatti, F. Kotsias, J. G. Magalhaes, S. Amigorena, Dendritic cell maturation and cross-presentation: timing matters! *Immunol. Rev.* **272**, 97–108 (2016).

90. F. Veglia, D. I. Gabrilovich, Dendritic cells in cancer: the role revisited. *Curr. Opin. Immunol.* **45** (2017), pp. 43–51.

91. A. Gardner, B. Ruffell, Dendritic Cells and Cancer Immunity. *Trends Immunol.* **37** (2016), pp. 855–865.

92. K. Palucka, J. Banchereau, Cancer immunotherapy via dendritic cells. *Nat. Rev. Cancer.* **12** (2012), pp. 265–277.

93. R. B. Mailliard *et al.*, α-type-1 polarized dendritic cells: A novel immunization tool with optimized CTL-inducing activity. *Cancer Res.* **64**, 5934–5937 (2004).

94. D. Zingg *et al.*, The Histone Methyltransferase Ezh2 Controls Mechanisms of Adaptive Resistance to Tumor Immunotherapy. *Cell Rep.* **20**, 854–867 (2017).

PUBLICATIONS

1. Nie L*, <u>Zhang Y*</u>, Dong W, et al. Involvement of zebrafish RIG-I in NF-κB and IFN signaling pathways: Insights into functional conservation of RIG-I in antiviral innate immunity (2015). Developmental & Comparative Immunology, 48(1): 95-101. *Co-First Author

2. Nie L, Xiong R, <u>Zhang Y</u>, et al. Conserved inhibitory role of teleost SOCS-1s in IFN signaling pathways (2014). Developmental & Comparative Immunology, 43(1): 23-29.

3. Wu M, Chen Y, Kim M, Chang C, Gampala S, <u>Zhang Y</u>, Wang Y, Chang C, Yang J, and Chang C. (2019). Epithelial-mesenchymal transition directs mammary stem cell fate via regulation of mitofusin. Cell Metabolism, 29(4):993-1002